INFORMATION TO USERS

CAD OF RECTANGULAR - RIDGED
WAVEGUIDE BANDPASS FILTERS

Carlos Alberto Andrade

A Thesis

In
The Department of

Electrical and Computer Engineering

Presented in Partial Fulfillment of the Requirements

For the Degree of Master of Applied Science

At Concordia University

Montreal, Quebec, Canada

April 2001

Canada

ABSTRACT

CAD OF RECTANGULAR-RIDGED
WAVEGUIDE BANDPASS FILTERS

Carlos Alberto Andrade

This thesis examines the design of rectangular or ridged waveguide bandpass filters using a computer. It studies the analysis of rectangular and ridged waveguide discontinuities using Mode-Matching (MM) and explains how to obtain the Generalized Scattering Matrix (GSM) form the MM analysis. Then, the thesis shows how to combine all the scattering matrices of a microwave circuit to obtain its overall scattering parameters of the circuit. The combination of the MM and GSM method allows the accurate and fast modeling of microwave bandpass filters with rectangular or ridged waveguide cross-sections. A Computer-Aid-Design (CAD) tool is built for the rigorous analysis of an evanescent-mode waveguide filter using the MM-GSM method. A Graphic-User-Interface (GUI) is part of the CAD tool. The user can enter filter parameters and analyze the accurate response of the filter within seconds. The thesis shows a particular design example of an evanescent-mode waveguide filter using the CAD tool. The filter dimensions found using the CAD tool were used to fabricate the filter. The filter was measured and compared with the simulated results. Good agreement between the two results was obtained.

ACKNOWLEDGEMENTS

I would like to thank Dr. Christopher Trueman for accepting to supervise me during this thesis. His advices were very helpful and are reflected throughout this thesis. His story about an old burger joint, "Where's the beef?", was always on my mind when writing the thesis. I would also like to thank all the professors of the Engineering Department of Concordia University for developing my knowledge, which allows me today to understand the physics and mathematics behind real world problems.

I would like to thank Jeff Joseph, manager at Mitec Telecom, for giving me my first work opportunity in the world of telecommunication. His enthusiasm inspired me to appreciate waveguides and, consequently, derive Maxwell's equations on the weekends. I would also like to thank Mitec Telecom for the valuable experience acquired during my four years in their facility. The evanescent-mode waveguide filter shown in this thesis was built and tested at Mitec and really enhances the thesis content. The convergence of a page-long expression derived from Maxwell's equations is always more tasteful when measurements confirm that the equation *works!*

I am very grateful to the two persons that are the most important to me in the world, my father, Alberto, and my mother, Helena. Without their financial and mental support, this thesis would not exist. Finally, I would like to thank my girlfriend, Catia, for surviving with me during this thesis. I promise you that I will keep my weekends free, ... until I find another academic challenge.

TABLE OF CONTENTS

LIST OF FIGURES

LIST OF TABLES

LIST OF ABBREVIATIONS

CAD   Computer-Aided Design

FDM   Finite-Difference Method

FEM   Finite-Element Method

MMM   Mode-Matching Method

MOM   Method of Moments

FDTD   Finite-Difference Time Domain

TLM   Transmission Line Method

GUI   Graphic-User-Interface

GSM   Generalized Scattering Matrix

IL   Insertion Loss

REJ   Rejection Requirements

RL   Return Loss

WG   Waveguide

TE   Transverse Electric

TM   Transverse Magnetic

BW   Bandwidth

CHAPTER 1 - Introduction

Microwave passive filters are essential components in the implementation of telecommunication systems. Their main purpose is to pass selected signals and attenuate unwanted signals. Thus, it can clean the communication network by letting only the system band signals to be transmitted or received.

The term *microwave* indicates that the device operates with alternating current signals with frequencies between 300 MHz and 300 GHz. At these frequencies, the electrical wavelength ranges from 1 mm to 1 m, which is comparable to the device size. Since the signal oscillates within the circuit physical length, the circuit dimensions, the signal amplitude and the signal phase must considered during the analysis of the device. This means that the general electromagnetic theory as described by the Maxwell's equations must be applied.

Microwave filters are generally made of transmission lines or waveguides. Common transmission lines used to build microwave filters are: stripline, microstrip line coaxial line, circular waveguide, rectangular waveguide, ridged waveguide and dielectric filled waveguide. Depending on the electric, mechanical and environmental specifications, some transmission lines offer better performance over the others. It is the microwave designer responsibility to be aware of all the transmission line properties so that the optimum filter performance is obtained.

Although the principals for microwave filter design were established approximately one century ago, microwave filter design remains an active research area today. Each year, many technical papers are still published by scientists and engineers on the new developments of microwave filter technology. The research has particularly increased over the last decade with the explosive growth of wireless and satellite telecommunication systems requiring higher performance and more reliable filter designs. An example is the implementation of new wireless digital telecommunication services at 38 GHz by Winstar Communications in New York, which offers the same quality services as the traditional wire line networks. But, because wireless network links can be set up in new locations more quickly, easily and at less cost, companies like Winstar are able to offer the same services at reduced rates. A few years ago, microwave filters at high frequency such as 38 GHz were impossible to manufacture due to the tight mechanical tolerances required and the lack of precise designing tools. Today, with the new advancements in machining and computer-aided design (CAD) tools, many telecommunication companies are manufacturing these filters.

The development of computers with fast processors, large memory and affordable pricing has considerably improved the way engineers design microwave filters. Originally, microwave filters were designed with empirical models and extensive tuning of the circuit in the laboratory. Most often, tuning elements (such as screws) were required, to permit experimental adjustment of the cavity resonances and intercavity couplings in order to obtain the desired filter response. The formulas derived were usually obtained from laboratory measurements or approximate solutions to field

equations and were introduced by the members of the MIT Radiation Laboratory [1] as well as by Matthaei, Young and Jones [2] shortly after the Second World War. Their work still remains a great contribution to the understanding and design of microwave passive components today. With the rapid improvement of computer performance in the twentieth century, the development of CAD tools based on the numerical solution of electromagnetic field equations emerged [3-4]. Numerical methods like Finite-Element Method, which approximates the field solution of the Maxwell's equations in a discrete space domain, gained a lot of popularity mainly because of the freedom it offers the microwave designer. Numerical method models are in general less limited in terms of space geometries or frequency ranges than empirical models. All the significant parameters of the microwave component can be taken into account. Furthermore, CAD tools based on the analysis of the field equations for a bounded geometrical problem has also considerably reduced pre-production time and cost of development of new microwave components which makes them much more attractive to the microwave industry. However, even today, because of machining and manufacturing tolerances, a very tight specification cannot be met by designing the filter with a rigorous numerical method and experimental tuning of the microwave filter is often still required.

Many numerical methods have been introduced in the past two decades to describe the scattering phenomena of waves inside microwave passive components. These numerical methods are often classified as space domain, modal domain or time domain method depending on the parameter that is being evaluated numerically (and usually truncated) when solving the field equations. Methods like Finite-Difference

Method (FDM) [5] and Finite-Element Method (FEM) [6] are examples of space discretization methods. Mode-Matching Method (MMM) [7] and Method of Moments (MOM) [8] are based on modal discretization, and Finite-Difference Time Domain (FDTD) [9] and Transmission Line Method (TLM) [10] belong to time and space discretization. A brief summary of each method is given in [3-4]. No matter to which class the numerical method belongs to, all the methods should converge to the same and unique solution of the four Maxwell's equations for the given boundary conditions of the component. In some technical papers, a lot of emphasis is placed on the advantages of one method over the other methods for a particular application. A good comparison between the different methods is usually done in terms of its computing requirements as shown by table 1.1 [3-4].

Table 1.1 - Comparison of Numerical Methods

Method	Storage	CPU	Versatility	Pre-processing
FDM	L	L	++	Nil
FEM	L	L	+++	+
TLM	L	L	++	+
MMM	S/M	S/M	+	++

Note : L = large, M = medium, S = small, +++ = very good, ++ = good, + = poor

In general, table 1.1 shows that space and time discretization methods require more memory storage and computer processing time than modal discretization methods.

However, space and time discretization methods are more versatile in the sense that they can analyse complex geometrical structures. Therefore, as a rule of thumb, it is usually preferred to use modal discretization methods over time and space discretization methods when the structure involved is of simple geometrical form because less memory and computing is required to converge to the solution.

Most of the CAD tools built today for the design of a microwave filter include more than just an electromagnetic field numerical solver. Often, CAD tools are combined with a synthesis algorithm, an optimization routine and a graphic-user-interface (GUI), which allows the user to enter data, direct instructions and display computational results. Therefore, CAD tool is a computer oriented process, which when the solver maintains enough convergence during the process, experimental tuning of the filter can be replaced by computer optimization of the circuit. A typical CAD tool flow diagram for a microwave filter design is illustrated in figure 1.1.

The process shown in figure 1.1 begins by stating the filter electrical specifications such as the insertion loss, return loss, passband and rejection band of the filter. If the filter initial dimensions are unknown, a synthesis method based on experimental data or approximation models can be used to obtain the initial filter dimensions. Once the initial (guess) dimensions are found, the numerical solver computes the filter response. After running the numerical analysis of the electromagnetic waves inside the filter, the computed response is compared with the specifications. If the filter fails to satisfy the given specifications, the filter dimensions are refined until all the

requirements are met. During the optimisation stage, the filter is analysed each time the filter dimensions are changed. It can take several iterations before the filter meets the requirements; hence the importance of selecting a fast numerical method for the solver. Finally, when the filter meets the specifications, the optimum filter dimensions found are used to fabricate the filter.
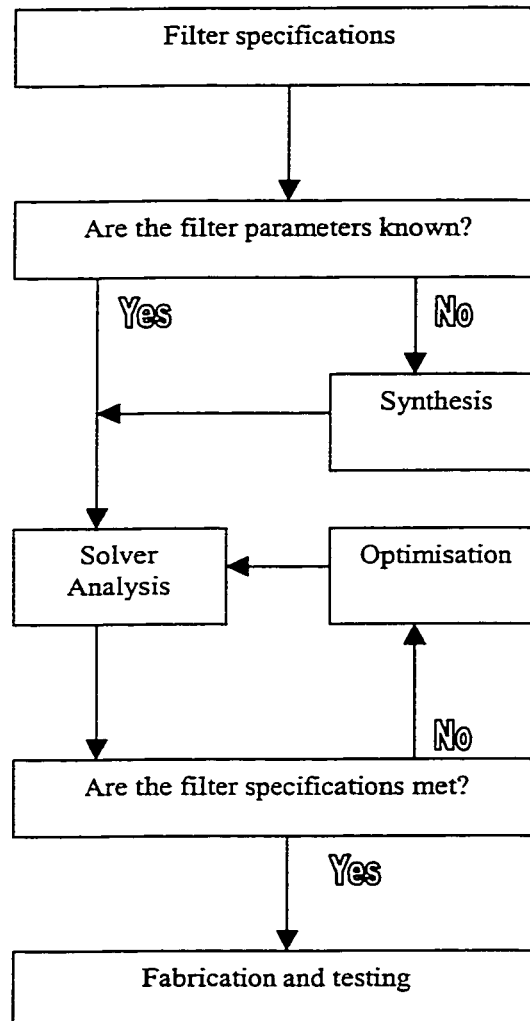
Figure 1.1 - CAD Flow Chart for a Microwave Filter Design

The objective of this thesis is to illustrate and apply the CAD process of figure 1.1 for the design of rectangular and ridged waveguide bandpass filters. All the key stages in the filter design will be addressed: the numerical analysis, the synthesis, the optimization as well as the fabrication and testing of the filter will be discussed.

Chapter two introduces the principals of microwave bandpass filter designs. It defines the common terms used in filter theory and states the objectives and challenges the designer needs to face during the design.

Chapter three presents the MMM based on [11-12] for the field analysis at the junction of two waveguides with dissimilar cross-sections. The waveguide discontinuities that will be studied in this chapter are: the rectangular-to-rectangular waveguide step and the rectangular-to-ridged waveguide step. Furthermore, it will be shown how to obtain a Generalised Scattering Matrix (GSM) for the waveguide step from the MM analysis.

Chapter four explains the decomposition of a microwave bandpass filter in terms of its GSMs. A GSM method will be presented to compute the overall GSM of the microwave filter. The combination of the two methods, MM-GSM, gives the complete field analysis of a rectangular-ridged waveguide bandpass filters and consequently, can be used to build the CAD solver.

Chapter five demonstrates the design of a microwave filter using the MM-GSM solver and the CAD process shown in figure 1.1. An evanescent-mode waveguide filter is synthesized, built and measured. The comparison between measured and simulated results will be discussed.

Finally, chapter six summarizes the work that was done and recommends further work to improve the design method.

CHAPTER 2 – Microwave Bandpass Filter Design

The subject of microwave filter design is very broad, due to the importance of these components in practical systems, and the variety of possible implementations. In this chapter, we treat only the basic implementation of a microwave bandpass filters. First, in section 2.1, the ideal bandpass filter response is discussed. The Chebyshev approximation to the ideal response follows in section 2.2. In section 2.3, we introduce some of the most popular filter design goals and solve for a Chebyshev filter response from given filter requirements. Finally, in section 2.4, we present the microwave realization of Chebyshev bandpass filters. For further explanation on each of these topics the reader is referred the classic tome of Matthaei, Young and Jones [2].

2.1   Ideal Microwave Filter

A microwave filter is a passive component used in microwave systems to control the frequency response of the system. Figure 2.1.1 shows the ideal frequency response of a bandpass filter. The transmitted power coefficient, P_T, is equal to one in the passband, frequencies between f_1 and f_2, whereas the transmitted power is equal to zero in the reject bands (i.e., the frequencies outside the passband region). This type of response is referred to be ideal because it is impossible in practice to obtain a lossless transmission in the passband and such a sharp transitions at f_1 and f_2. Many factors contribute to make the microwave filter to be non-ideal such as the finite property of the materials, the finite

number of periodical resonators, machining tolerances, manufacturing tolerances and variable environmental conditions.
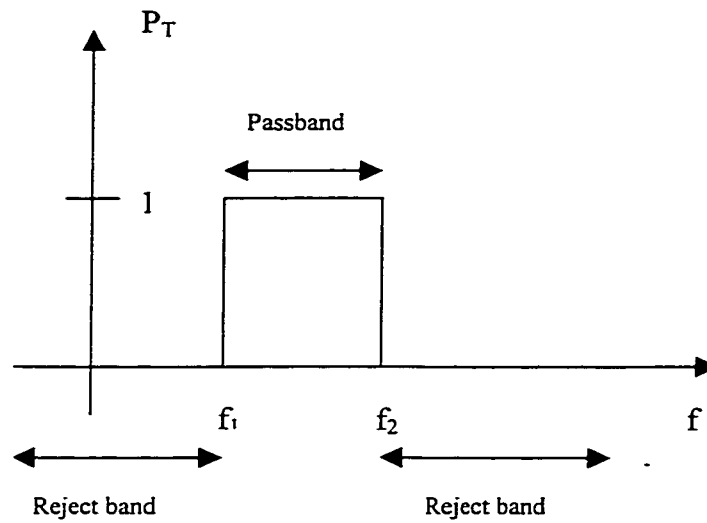
Figure 2.1.1 - Ideal Bandpass Filter Response

2.2   Chebyshev Filter Approximation

The first step in the filter design consists on selecting a characteristic function that approximates the ideal filter response shown in figure 2.1.1. Many transfer functions exist [13], but in this thesis only the Chebyshev (or equal-ripple) approach will be considered. For a Chebyshev bandpass filter, the transmitted power is defined by

$$P_T = \frac{1}{1 + k^2 T_N^2 \left(\frac{f_0}{(f_2 - f_1)} \left(\frac{f}{f_0} - \frac{f_0}{f} \right) \right)}$$

(2.2.1)

where T_N is the Nth degree Chebyshev polynomial of the first kind, $1/(1+k^2)$ is the passband ripple and $f_0=\text{sqrt}(f_2 \cdot f_1)$. Figure 2.2.1 shows a 4th order Chebyshev bandpass filter response. For a 4th order Chebyshev bandpass filter, the transmission response will have exactly four frequencies in the passband at which the filter will have perfect transmission (if the filter is lossless). These four frequencies are spaced from each other in the passband such that the transmitted power of the filter oscillates between 1 and $1/(1+k^2)$ in the passband. In the reject band the power transmission is attenuated monotonically, which means that the attenuation curve has no sudden discontinuity or ripples.
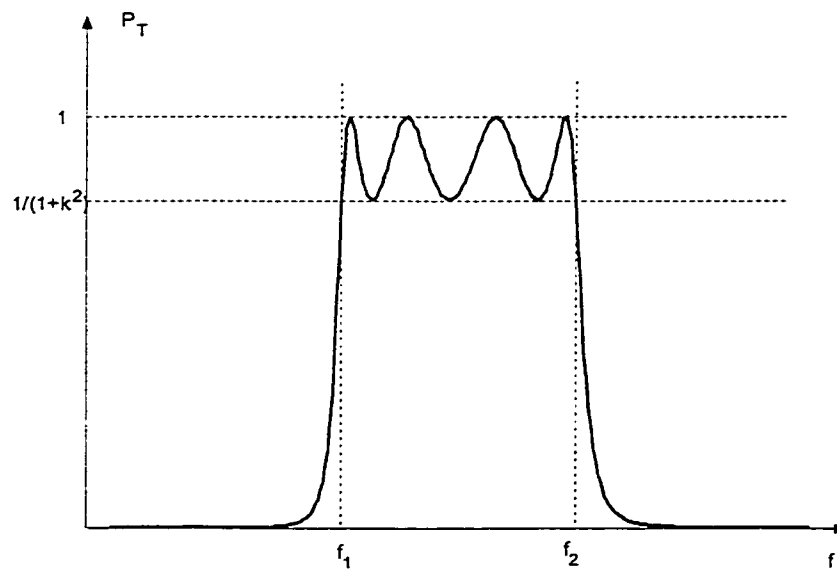
Figure 2.2.1 - 4th Order Chebyshev Bandpass Filter Response

Figure 2.2.2 compares two Chebyshev bandpass filter responses. The dotted line response has k=0.5 and N=3 whereas the solid line response has k=0.1 and N=9. The solid line response is much closer to the ideal response. Therefore, the Chebyshev

response with lower k and higher N approximates better the ideal response. In fact, if k would tend to zero and N would tend to infinity, the Chebyshev response would tend to the ideal bandpass filter response. This is why the Chebyshev response is called an approximation method. In practice, k cannot tend to zero nor can N tend to infinity. Therefore, the objective of the filter designer is to find k and N such that the filter meets specific requirements.
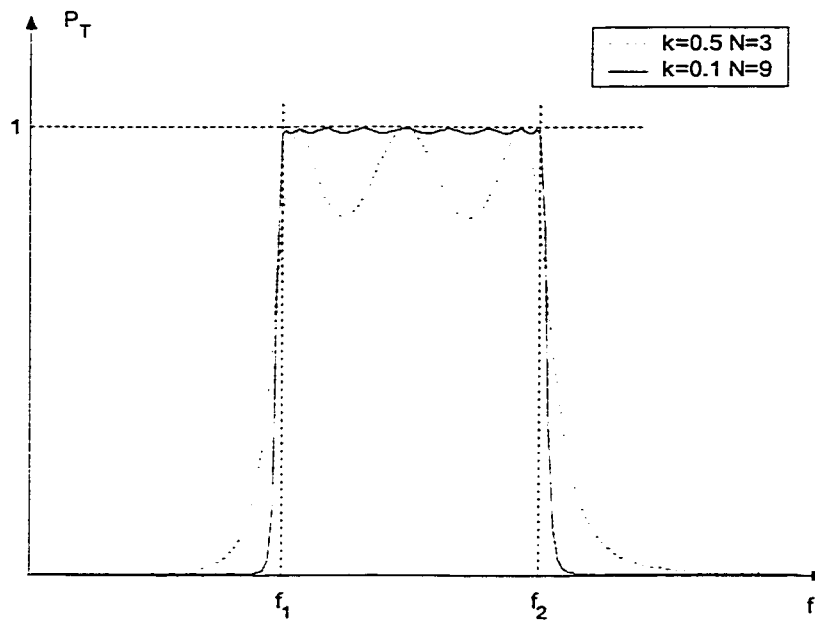
Figure 2.2.2 - Chebyshev Bandpass Filter Responses With Different k and N

2.3 Filter Design Requirements

A microwave filter is a two-port network as shown in figure 2.3.1. The input port of the filter is connected to a source impedance, Z_s, and the output port to a load

impedance, Z_L. Because microwave waves can travel back and forth in a given direction, it makes sense to express the quantities observed at the two ports as a reflection wave coefficient or a transmission wave coefficient rather than a voltage or a current. Therefore, a common mathematical representation of this network response is given by the scattering matrix, S(f),

$$S(f) = \begin{bmatrix} S_{11}(f) & S_{12}(f) \\ S_{21}(f) & S_{22}(f) \end{bmatrix}$$

(2.3.1)

where S_{ij} repesents the magnitude and phase of the wave measured at port i if the network is excited by a normalized wave at port j. Therefore, S_{11} and S_{22} measures the

Port 1   Port 2

Two-Port
Network
S(f)

Z_s Z_L
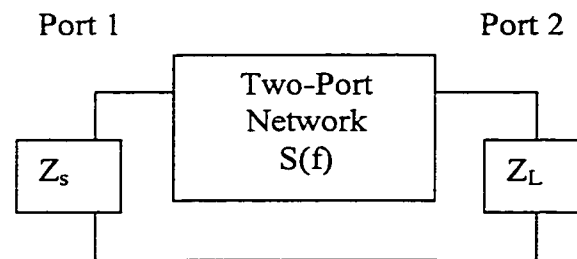
Figure 2.3.1 - Two-port Network

wave reflection at port 1 and port 2 respectively, S_{12} measures the wave transmission from port 2 to port 1 and S_{21} measures the wave transmission from port 1 to port 2. The relationship between transmission coefficient and the power transmission coefficient is given by

$$P_T = |S_{21}|^2 = |S_{12}|^2 \qquad (2.3.2)$$

Filter magnitude requirements are often expressed in decibels, dB, and can be extracted from the scattering matrix. For example, the insertion loss, IL, measures the total attenuation in the signal after the signal passes through the filter and is related to the scattering matrix by

$$IL = 10 \cdot \log\left(\frac{1}{|S_{21}|^2}\right) \qquad (2.3.3)$$

The rejection requirements, REJ, of a filter are also defined by equation (2.3.3), but the insertion loss is a passband requirement whereas the rejection is a reject band requirement. Another common magnitude requirement is the return loss which measures the input and output match of the network to the characteristic impedance of the medium. The return loss at port 1, for example, is defined as

$$RL = 10 \cdot \log\left(\frac{1}{|S_{11}|^2}\right) \qquad (2.3.4)$$

Like the insertion loss, the return loss requirement is usually defined over the passband of the filter.

Once the filter requirements are defined, the goal of the filter design consists of finding the minimum order, N, and maximum ripple, k, in order to minimize the insertion loss, IL, maximize return loss, RL, and maximize rejection, REJ of the filter response. For example, if the requirement in the passband is defined as IL < 1 dB and RL > 10 dB over the frequency range, 10 < f < 12 GHz, and in the reject band is defined by REJ > 25 dB for 8 < f < 9 GHz and 13 < f < 14 GHz. Using equation (2.2.1), we find that the minimum Chebyshev order is N=4 and maximum ripple is k=0.33 to meet the amplitude requirements. Figure 2.3.2 illustrates this example. If the order would be less than 4 or the ripple more than 0.33, the filter would not meet all the requirements. On the other hand, if the order of the filter is greater than 4 and the ripple less than 0.33, the filter would still meet the specifications with more margin. The tradeoff on how much margin to allow when designing a microwave filter is probably the most difficult task the filter designer has to face. This information can only be estimated from experience with past designs because many unpredictable phenomena such as machining variance, manufacturing processes and variable environmental conditions can affect the filter performance. Allowing too much margin in the design increases the cost of fabrication of the filter and can lead to the loss of the contract if the other filter suppliers can meet the requirements with a lower cost unit. However, too tight margins may cause the filter to fail some of the filter requirements under environmental conditions and, consequently, the loss of the contract.
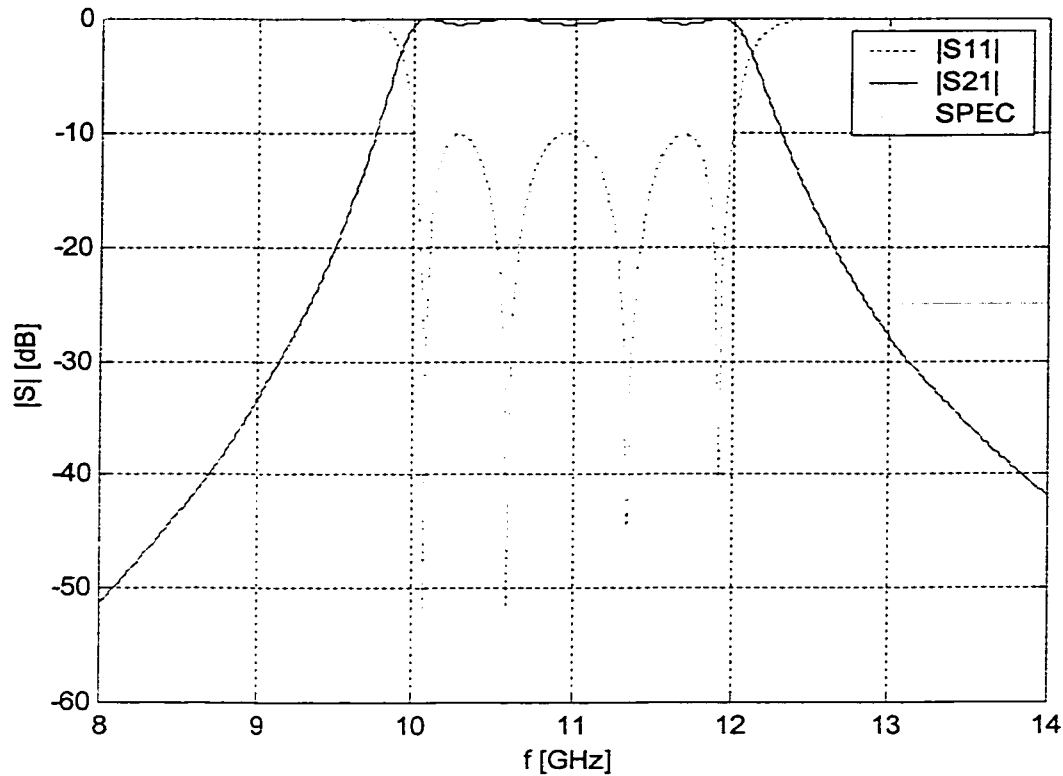
Figure 2.3.2 - Chebyshev Bandpass Filter with N=4 and k=0.33.

Once the Chebyshev filter order and ripple is known, to arrive at a prescribed frequency response, the designer needs to synthesize a two-port network that will match the frequency response required. In the case of a microwave networks, synthesis consists of determining the physical dimensions of the transmission lines or waveguides.

2.4   Microwave Filter Synthesis

The most popular synthesis method used in microwave Chebyshev bandpass filter designs is probably the direct-coupled-resonator method. Cohn [14] introduced the method in 1957 for the design of inductive coupled rectangular waveguide filters and capacitively coupled microstrip filters. Matthaei, Young and Jones [2] and Uher [15] use the same approach for many other microwave bandpass filter designs.

The direct-coupled-resonator method begins by the two-port lowpass Chebyshev network shown in figure 2.4.1. The lowpass elements, g_i, are in fact lumped element components. In figure 2.4.1, for i equal to an odd number, g_i is a series inductor and for i equal to even numbers, g_i is a shunt capacitor. Also, depending if the filter order is even or odd, the circuit will terminate with a shunt capacitor or a series inductor as shown in figure 2.4.1 (a) and (b) respectively. The lowpass elements are derived from the Chebyshev filter ripple, k, the order, N, and the following equations,

$$g_1 = \frac{2a_1}{\gamma} \tag{2.4.1}$$

$$g_i = \frac{4a_{i-1}a_i}{b_{i-1}g_{i-1}} \quad ,i = 2,3...N \tag{2.4.2}$$

$$a_i = sin\left(\frac{(2i-1)\pi}{2N}\right) \quad ,i = 1,2,...N \tag{2.4.3}$$

$$b_i = \gamma^2 + sin^2\left(\frac{i\pi}{N}\right) \quad ,i = 1,2,...N \tag{2.4.4}$$

$$\gamma = sinh\left(\frac{\beta}{2N}\right)$$
(2.4.5)

$$\beta = ln\left[\frac{coth\left(10log\left(1 + k^2\right)\right)}{17.37}\right]$$
(2.4.6)

(a) N is even

(b) N is odd
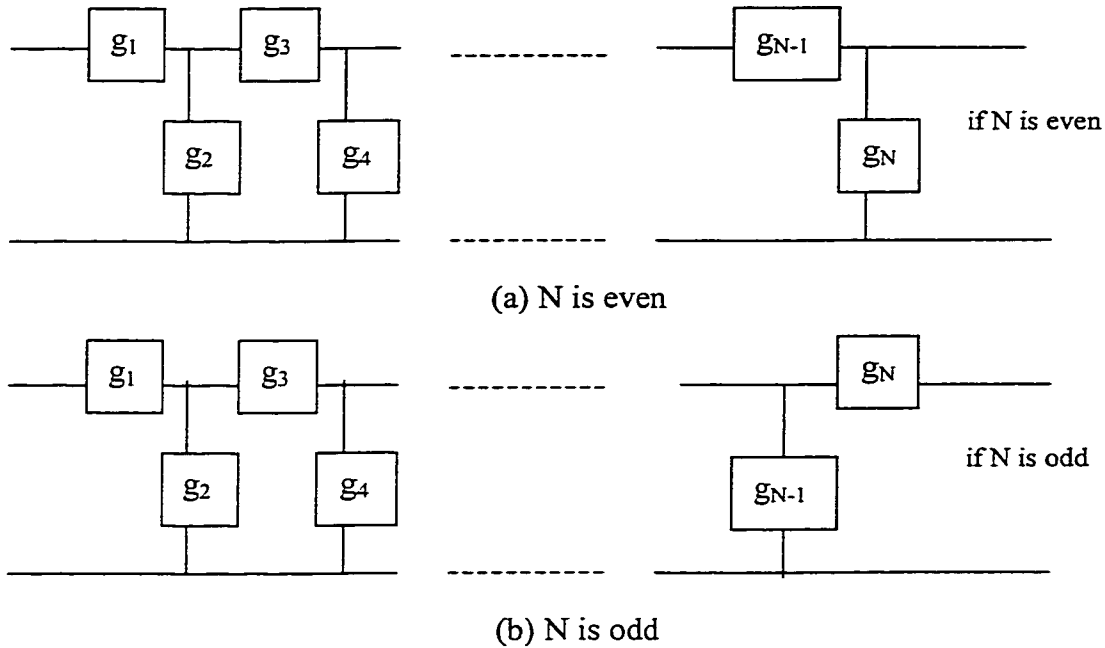
Figure 2.4.1 - Chebyshev Prototype

The Chebyshev bandpass filter is obtained from the lowpass network through a transformation. The lowpass to bandpass filter transformation consists of replacing the series elements in figure 4.2.1 by series LC resonators where

$$L_i = \frac{g_i}{2\pi f_0 \Delta} \quad , i = 1,3,5,...$$
(2.4.7)

$$C_i = \frac{\Delta}{2\pi f_0 g_i} \quad , i = 1,3,5,...$$
(2.4.8)

and replacing the shunt elements in figure 4.2.1 by parallel LC resonators where

$$L_i = \frac{\Delta}{2\pi f_0 g_i} \quad ,i = 2,4,6,\ldots$$

(2.4.9)

$$C_i = \frac{g_i}{2\pi f_0 \Delta} \quad ,i = 2,4,6,\ldots$$

(2.4.10)

where $f_0 = \sqrt{f_1 \cdot f_2}$ and $\Delta = (f_2 - f_1) / f_0$. A Chebyshev bandpass filter with alternate series and parallel microwave resonators is difficult to realize. Therefore, another transformation is required to bring all the resonators into series resonators. This transformation is done, by introducing impedance inverters (K-inverter circuits) between the series and parallel resonators. Looking into its input port, a K-inverter circuit inverts and scales the load impedance connected to its output port. Therefore, the Chebyshev network can be transformed into an impedance inverter circuit shown in figure 2.4.2. The series LC resonators are shown in terms of their reactance, X_i, in figure 2.4.2. All the resonators are now in series, interconnected with K-inverters. The elements of the impedance inverter network are given by

$$K_{01} = \sqrt{\frac{2\pi f_0 \Delta L_1^p Z_s}{g_1}}$$

(2.4.11)

$$K_{i,i+1} = 2\pi f_0 \Delta \sqrt{\frac{L_i^p L_{i+1}^p}{g_i g_{i+1}}} \quad ,i = 1,2,\ldots,N-1$$

(2.4.12)

$$K_{N,N+1} = \sqrt{\frac{2\pi f_0 \Delta L_N^p Z_L}{g_N}}$$

(2.4.13)

$$X_i(f) = 2\pi f L_i^p - \frac{1}{2\pi f C_i^p} \quad , i = 1, 2, \ldots, N \qquad (2.4.14)$$

$$L_i^p C_i^p = \frac{1}{\sqrt{2\pi f_0}} \qquad (2.4.15)$$
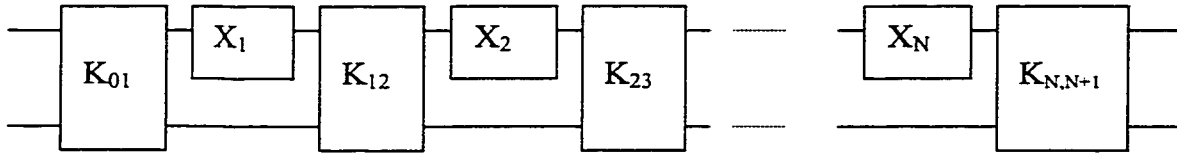
Figure 2.4.2 - Impedance Inverter Bandpass Network

This impedance inverter network is much easier to realize with microwave circuits since a half wavelength waveguide, for example, can behave like a series LC resonator and the coupling between waveguide resonators through small apertures (irises) can behave like a K-inverter. Therefore, a direct-coupled rectangular waveguide bandpass filter as shown in figure 2.4.3 can be directly matched to a Chebyshev impedance inverter network. The iris dimensions can be found from the amount of coupling (or, K-inverter) between the resonators. The higher the coupling is required the bigger the iris opening will be. The waveguide resonator lengths will be slightly less than a half wavelength to include the electromagnetic field perturbation in the cavity due to the coupling apertures. Using experimental data or a fullwave solver, the iris widths, L_{ci}, and resonator lengths, L_{ri}, can be found for the bandpass microwave filter at a given frequency. Usually, the center frequency, f_0, is chosen to synthesize the network in order to achieve a good impedance match in the passband.
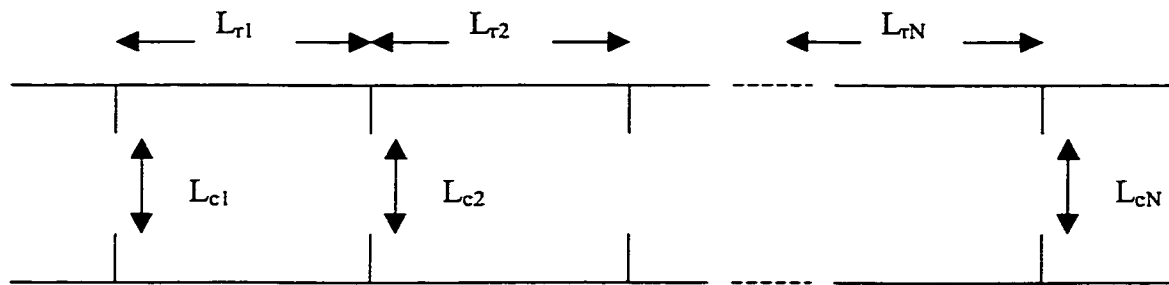
Figure 2.4.3 - Direct-Coupled Rectangular Waveguide Bandpass Filter

The direct-coupled-resonator synthesis method can be used for any waveguide resonators coupled by evanescent waveguide sections. The method is very accurate for bandpass filters with a percentage bandwidth, Δ, less than two percent. However, for wider passband filters the model still predicts a good matching at the center frequency but decreases in accuracy as we deviate from the center frequency. Therefore, to obtain a good return loss over the whole passband the filter dimensions must be refined. Traditionally, the filter refinement consisted of using tuning screws to optimize the resonators and the intercavity irises. Today, optimization of the microwave filter is often done using a fullwave solver. However, if tight filter specifications are required, it is still economical to use tuning screws on the resonators and irises to compensate for the manufacturing errors.

CHAPTER 3 – Mode Matching Method

The Mode Matching Method (MMM) is often used to solve boundary-value problems involving waveguides. The method consists of decomposing a complex geometrical structure into many regions of simple geometrical form. Hence, in each region, we can find a set of modal functions (or, modes) that satisfy the Maxwell's equations except at the junctions. Then, the problem consists of expanding all the modes in each region with unknown modal coefficients and solving for these coefficients by applying the boundary conditions at the junction of each region.

The MMM can be formulated to solve for the scattering parameters of waveguide discontinuities. Publications on the subject exist since 1944. However, it was only in 1967, with Wheeler [7], that the method was finally formulated in a systematic way to solve for the scattering of waveguide steps. Since then, MMM has been applied to the scattering analysis of many microwave components such as direct-coupled-resonators filters [11], step transformers [12] and couplers [16].

In addition to waveguide scattering problems, the MMM can be used to solve eigenvalue problems. In other words, it can be formulated to obtain the resonant frequency of microwave cavities and the cutoff frequencies of waveguides. Some very complex eigenvalue problems have been solved by MM such as dielectric resonator (DR) cavities [17] and microstrip lines [18].

In this chapter, both the scattering and eigenvalue problems will be demonstrated and solved by MMM. In section 3.1, a 3-D rectangular waveguide discontinuity problem is simplified to a 1-D problem in order to reduce the mathematical complexity of the solution and focus on the MM principles. In section 3.2, the same rectangular-to-rectangular waveguide step is solved by MM for the scattering parameters, but this time, the method is applied rigorously using all the waveguide modes and boundary conditions. The formulas that will be derived in this section are based on [12] and are valid for waveguide steps with any cross-section geometry. Therefore, the formulas will be used again in section 3.3 for the scattering analysis of a rectangular-to-ridged waveguide step. However, the wave numbers (or eigenvalues) of the ridged waveguide cannot be solved exactly from Maxwell's equations and MM will be used to solve numerically for these wave numbers.

3.1   Simple Example

A simple one dimensional boundary condition problem will be solved in this section by the MMM in order to illustrate the principle of the MMM.   In reality, the boundary condition problem between two dissimilar waveguides as shown in figure 3.1.1 cannot be rigorously analyzed as a one-dimensional problem, but this will be done in this section in order to reduce the mathematical complexity and focus on the fundamental concepts of the MMM.

The discontinuity between two rectangular waveguides is shown in figure 3.1.1. In the first waveguide, wg-I, a y-directed electric field is excited and travels in the positive z-direction towards the second waveguide, wg-II. Assuming that only the fundamental mode operates in wg-I with a maximum amplitude of one and that the y-directed fields in the waveguides have no y and z dependence, the problem consists of finding the electric field in the second waveguide at the discontinuity (z=0) when the excited electric field in wg-I arrives at the discontinuity.
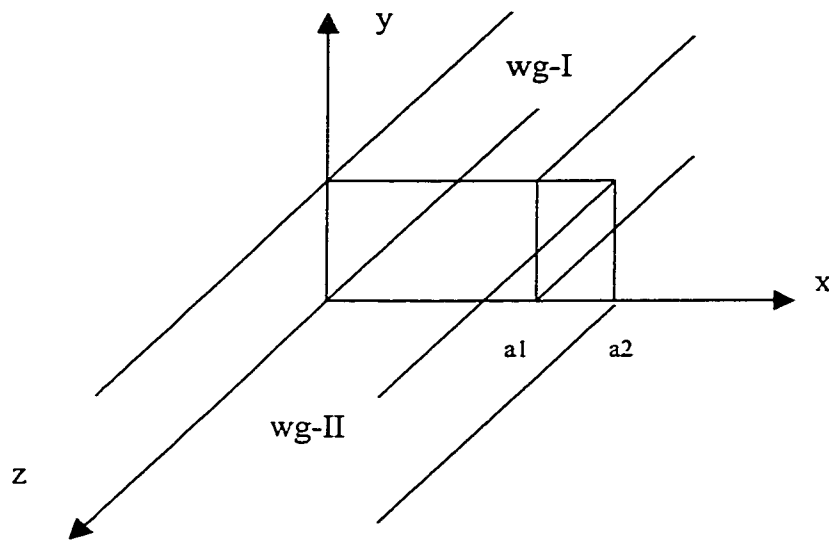
Figure 3.1.1 - Discontinuity Between Two Rectangular Waveguides

The first step in the MMM consists decomposing the complex structure into two waveguide rectangular sections, wg-I and wg-II. Then, in each waveguide, the wave equation and the boundary conditions must be solved to find all the possible solutions or

modes.   For an x-varying y-directed electric field, the wave equation in the two waveguides can be expressed by

$$\left(\frac{d}{dx^2}^2 + k_c^{\,2}\right)E_y^v = 0 \tag{3.1.1}$$

where $v = $ I or II for wg-I and wg-II respectively and the cutoff wave number, k_c. The general solution to the wave equation in (3.1.1) is

$$E_y^v(x) = c_a^v cos(a^v x) + c_b^v sin(b^v x) \tag{3.1.2}$$

where c_a and c_b are constant coefficients and a and b are the cross-section wave numbers. Now, (3.1.2) must be solved subject to the boundary conditions of the specific guide geometry.   In this problem, a metallic wall exists at $x = 0$ and $x = a_1$ for wg-I and $x = 0$ and $x = a_2$ for wg-II. Since E_y is tangential to the metal walls, (3.1.2) must vanish at the wall surfaces. Therefore,

$$E_y^I(0) = 0 \quad \Rightarrow \quad c_a^I = 0$$

$$E_y^I(a_1) = 0 \quad \Rightarrow \quad b^I = \frac{m\pi}{a_1}$$

$$E_y^{II}(0) = 0 \quad \Rightarrow \quad c_a^{II} = 0$$

$$E_y^{II}(a_2) = 0 \quad \Rightarrow \quad b^{II} = \frac{m\pi}{a_2}$$

where m = 1, 2, 3 ....   The exact solution to the wave equation and boundary conditions in both guides is then

$$E_y^I(x) = c_m^I sin\left(\frac{m\pi}{a_1}x\right) \tag{3.1.3}$$

and

$$E_y^{II}(x) = c_m^{II} \sin\left(\frac{m\pi}{a_2}x\right)$$

(3.1.4)

where c^I and c^{II} are the amplitude coefficients and the mode numbers, m = 1, 2, 3 ....

The amplitude coefficients in (3.1.3) are known since the problem states that only the

fundamental mode propagates in wg-I with an amplitude coefficient of one. Therefore,

$c^I_1 = 1$ and $c^I_m = 0$ for m = 2, 3, 4 ... and the exact y-directed electric field in wg-I is

given by

$$E_y^I(x) = \begin{cases} \sin\left(\dfrac{\pi}{a_1}x\right) & ,0 \le x \le a_1 \\ 0 & ,elsewhere \end{cases}$$

(3.1.5)

In the second waveguide, the exact y-directed electric field can be expressed as the sum

of all wave modes by

$$E_y^{II}(x) = \begin{cases} \displaystyle\sum_{m=1}^{\infty} c_m^{II} \sin\left(\dfrac{m\pi}{a_2}x\right) & ,0 \le x \le a_2 \\ 0 & ,elsewhere \end{cases}$$

(3.1.6)

In (3.1.6), the amplitude coefficients, c^{II}_m, are unknown and must be solved by matching

the tangential fields at the junction of wg-I and wg-II by

$$E_y^{II}(x) = \begin{cases} E_y^I(x) & ,0 \le x \le a_1 \\ 0 & ,elsewhere \end{cases}$$

(3.1.7)

Substituting (3.1.5) and (3.1.6) into (3.1.7) gives

$$\sum_{m=1}^{\infty} c_m^{II} sin\left(\frac{m\pi}{a_2}x\right) = sin\left(\frac{\pi}{a_1}x\right) \qquad ,0 \leq x \leq a_1 \qquad (3.1.8)$$

In order to solve for the coefficients, $c^{II}{}_m$, it is necessary to remove the x dependence in

equation (3.1.8). This can be done by multiplying both sides of (3.1.8) by $sin(n\pi x/a_2)$ and

integrating both sides over $0 < x < a_2$,

$$\int_0^{a_2} \sum_{m=1}^{\infty} c_m^{II} sin\left(\frac{m\pi}{a_2}x\right) sin\left(\frac{n\pi}{a_2}x\right) dx = \int_0^{a_1} sin\left(\frac{\pi}{a_1}x\right) sin\left(\frac{n\pi}{a_2}x\right) dx \qquad (3.1.9)$$

Using the orthogonality principle, equation (3.1.9) can be simplified to

$$c_m^{II} \frac{a_2}{2} = \int_0^{a_1} sin\left(\frac{\pi}{a_1}x\right) sin\left(\frac{m\pi}{a_2}x\right) dx \qquad (3.1.10)$$

Therefore, the amplitude coefficients in wg-II are given by

$$c_m^{II} = \frac{2}{a_2} \left[\frac{sin\left(\left(\frac{\pi}{a_1}-\frac{m\pi}{a_2}\right)a_1\right)}{2\left(\frac{\pi}{a_1}-\frac{m\pi}{a_2}\right)} - \frac{sin\left(\left(\frac{\pi}{a_1}+\frac{m\pi}{a_2}\right)a_1\right)}{2\left(\frac{\pi}{a_1}+\frac{m\pi}{a_2}\right)} \right] \qquad (3.1.11)$$

Substituting (3.1.11) into (3.1.6) gives us the exact solution to the problem. However, the

series in (3.1.6) uses an infinite number of terms, which is mathematically impossible to

compute. Truncation of the series to a total of M terms can be use to approximate the

exact solution.

In order to demonstrate the convergence of the method to the exact solution,

figure 3.1.2 (a), (b) and (c) shows the electric field in wg-I and wg-II at the discontinuity

given that $a_1 = 0.6$ and $a_2 = 1$ for $M = 3$, $M = 6$ and $M = 15$ respectively.
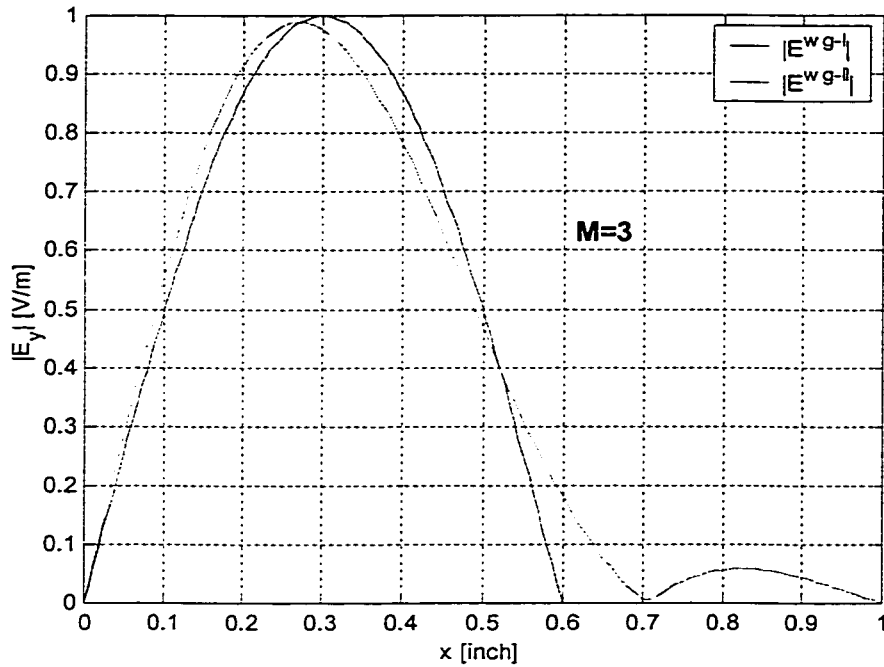
(a) M=3
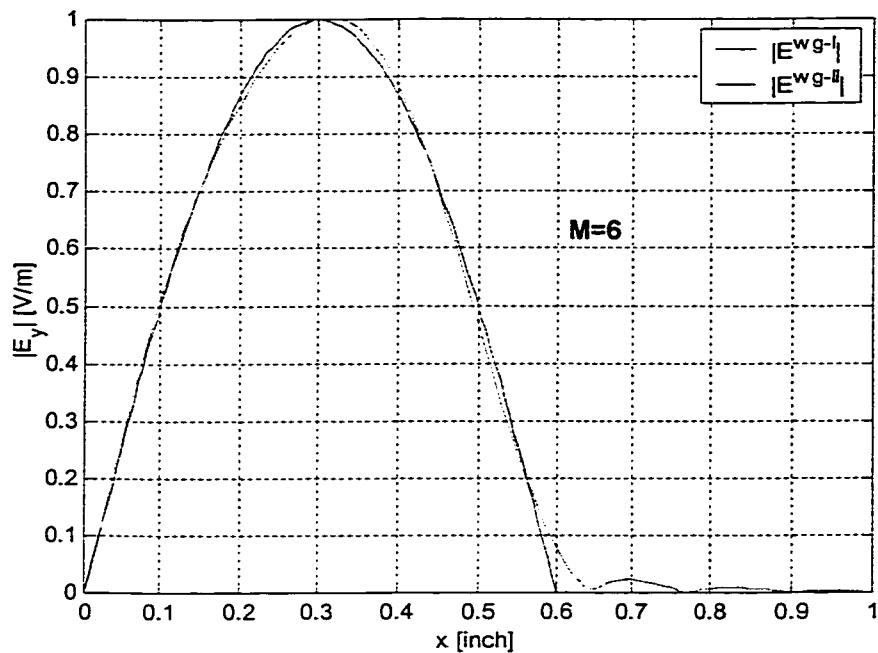
(b) M=6
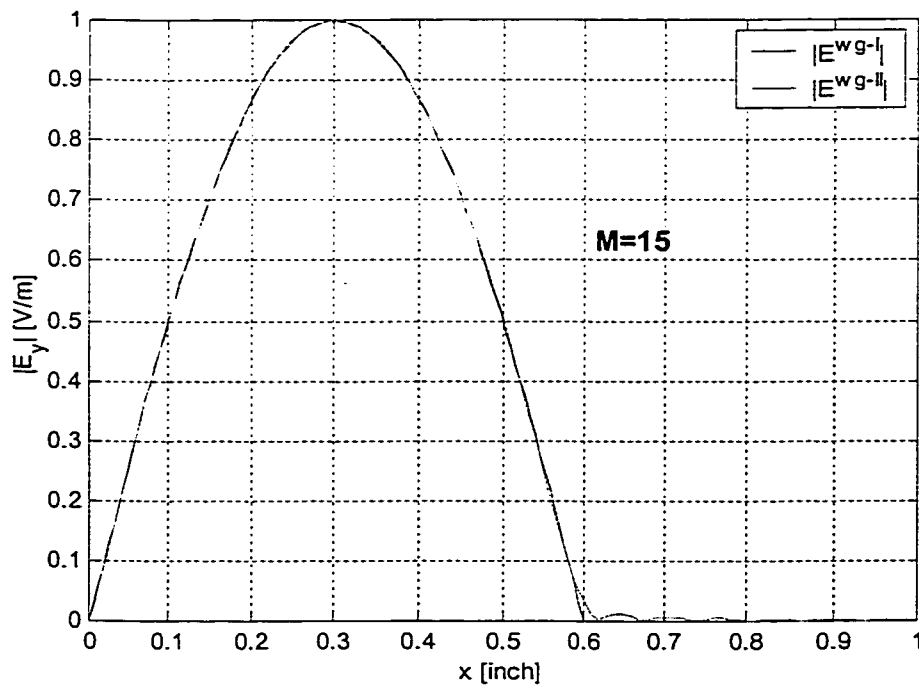
(c) M=15

Figure 3.1.2 - Electric Fields at the discontinuity For Different M terms.

Figure 3.1.2 shows that the mode matching solution converges to the exact solution, which is imposed by the boundary condition stated in equation (3.1.7). As M increases, the two electric field expressions are better matched over $0 \le x \le 0.6$ and the metallic boundary condition for wg-II over $0.6 \le x \le 1$ is also better respected.

The convergence of the method can also be verified numerically. In this example, the exact solution is known and a convenient error function due to the truncation of the series to M terms can be defined by,

$$E(M) = \int_0^{0.6} \left\| E_y''(x, M) \right| - \left| E_y'(x) \right\| dx + \int_{0.6}^1 \left| E_y''(x, M) \right| dx \qquad (3.1.12)$$

Equation (3.1.12) was computed for $3 \le M \le 22$. The results are shown in table 3.1.1, which shows that the error, E, tends to zero as M tends to infinity. The graphical representation of table 3.1.1 is shown in figure 3.1.3.

Table 3.1.1 - Error by Truncating the Series to M Terms

M	E
3	0.050720
4	0.021756
5	0.021756
6	0.013147
7	0.010243
8	0.009739
9	0.006787
10	0.006787
11	0.005151
12	0.004323

13	0.004278
14	0.003413
15	0.003413
16	0.002834
17	0.002478
18	0.002491
19	0.002107
20	0.002107
21	0.001802
22	0.001590
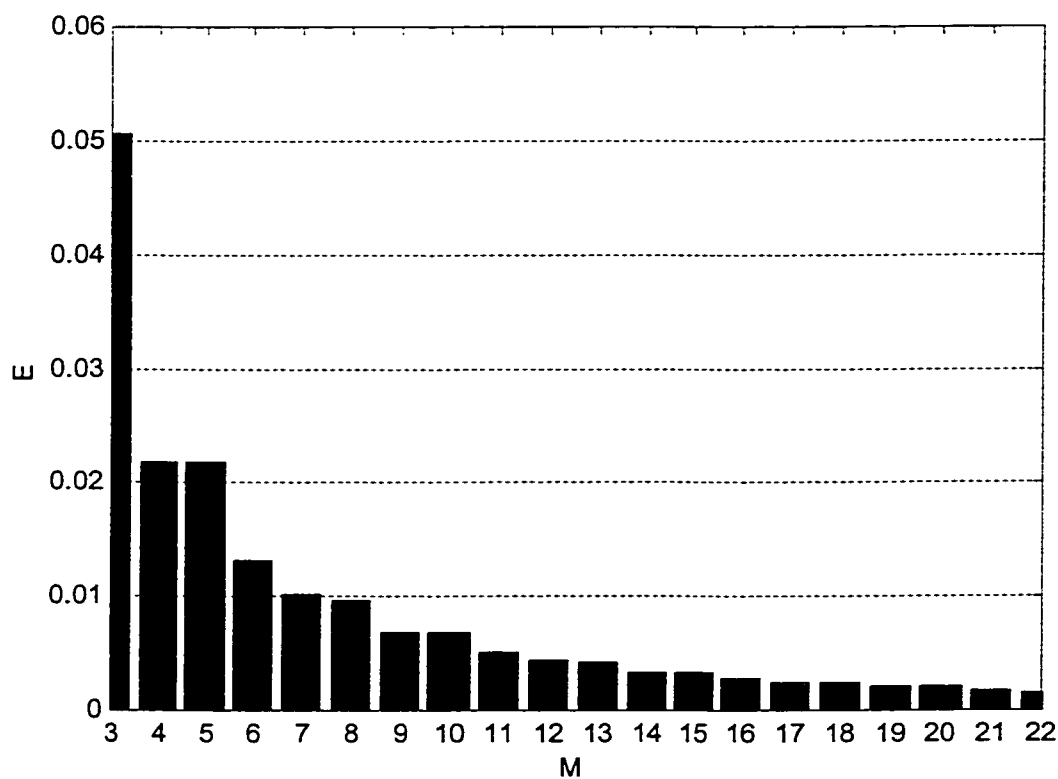
Figure 3.1.3 - Error function over M

In most numerical problems, the exact solution is unknown. The solution

accuracy is then determined by observing that the sequence of solutions obtained, as we

increase M, tends toward a value. For example, we can observe the y-directed electric

field intensity in wg-II at x = 0.7 for example. Table 3.1.2 and figure 3.1.4 shows the results obtained for $3 \leq M \leq 22$. In this case, we observe an oscillating convergence of $|E_y|$ at x = 0.7 due to the position of the nulls. For example, figure 3.1.2 (a), M = 3, shows that $|E_y|$ at x = 0.7 is very close to a null whereas figure 3.1.2 (b), M = 6, $|E_y|$ at x = 0.7 is between two nulls. Also shown in figure 3.1.2 is that as we increase M more nulls are placed in the metal boundary region of $0.6 \leq x \leq 1$, if M would tend to infinity, an infinity number of nulls would be placed in that region, which would tend $|E_y|$ in wg-II to the exact solution, which is $|E_y| = 0$ at x =0.7. Hence, as M increases the oscillations in the $||E_y|$ sequence reduce and the solution tends more and more to the exact solution.

Table 3.1.2 - $|E_y|$ at x=0.7 in wg-II for $3 \leq M \leq 22$

M	$|Ey(x=0.7)|$
3	0.0049
4	0.0400
5	0.0400
6	0.0221
7	0.0263
8	0.0166
9	0.0062
10	0.0062
11	0.0008
12	0.0050
13	0.0038
14	0.0069
15	0.0069
16	0.0045
17	0.0052
18	0.0033
19	0.0011
20	0.0011
21	0.0008
22	0.0020
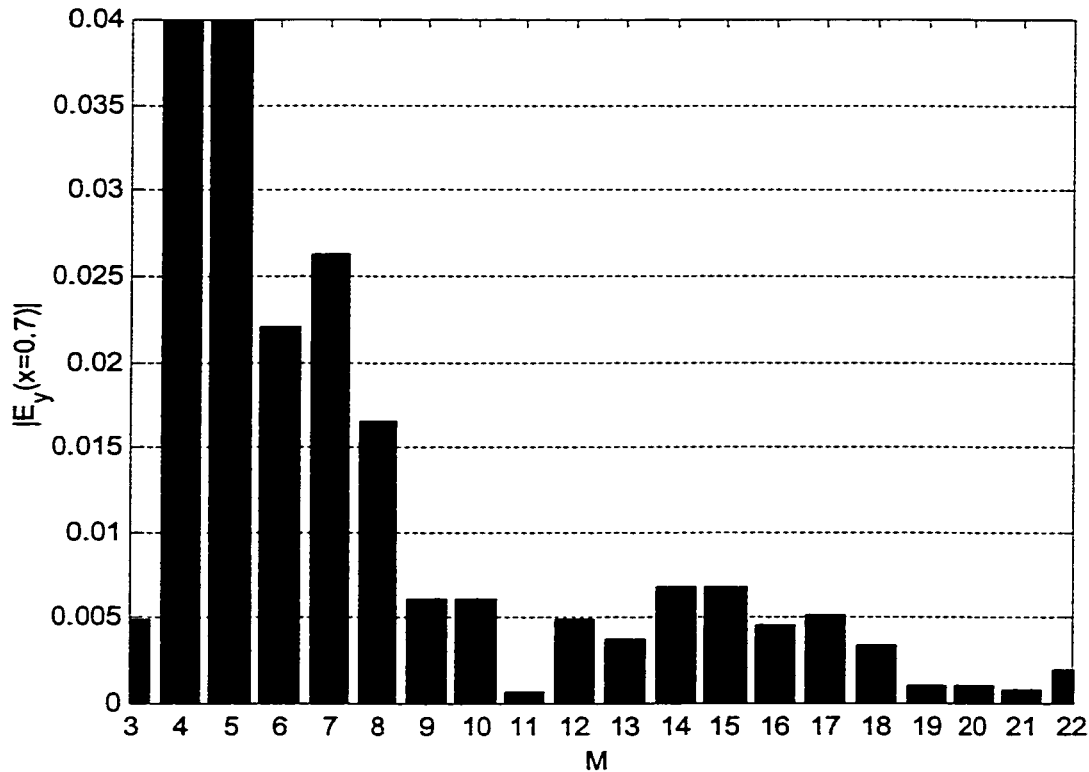
Figure 3.1.4 - Magnitude of E_y in wg-II at x = 0.7 versus M

This example was used to introduce the basic concepts of the MMM to solve a one-dimensional boundary condition problem. First, the exact field equations inside wg-I and wg-II, (3.1.5) and (3.1.6), were found from the wave equation (3.1.1) and the metal boundary conditions of each waveguide cross-section. Then, given that the wave in wg-I is known at the junction of the two dissimilar waveguides, the unknown amplitude coefficients in (3.1.6) were found by matching the tangential fields at the discontinuity by (3.1.7). The exact solution, (3.1.6), is an infinite series of sinusoidal terms (or modal functions) and can be truncated in order to be computed. By truncating the series to M terms the solution is no longer exact. Enough M terms must be used in order to achieve a

solution with a certain precision. The more the precision requirements are the more M terms must be used in the series expansions.

In the following sections of this chapter, the same mode matching analysis will be applied but this time the mathematical expressions will be more complex in order to include all the 3-D boundary conditions of the problem. First, the 2-D wave equation will be solved in each waveguide cross-section to obtain the electric and magnetic field expressions. Then, the 3-D boundary problem between two dissimilar waveguides will be analyzed by matching the tangential fields at the discontinuity based on theory given in [11] and [12]. Two discontinuity waveguide steps will be analyzed by the MMM, namely the symmetrical rectangular-to-rectangular waveguide step and the symmetrical rectangular-to-ridged waveguide step.

3.2   Symmetrical Rectangular-to-Rectangular Waveguide Step

A symmetrical rectangular-to-rectangular waveguide step discontinuity is formed when two rectangular waveguides with different cross-sections are joined as shown in figure 3.2.1. The discontinuity formed is said to be symmetric because both waveguides are centered at the origin (i.e., at x = 0 and y = 0). Before finding all the electric and magnetic fields solutions in both waveguide sections an explanation on the use of the symmetry will be given.
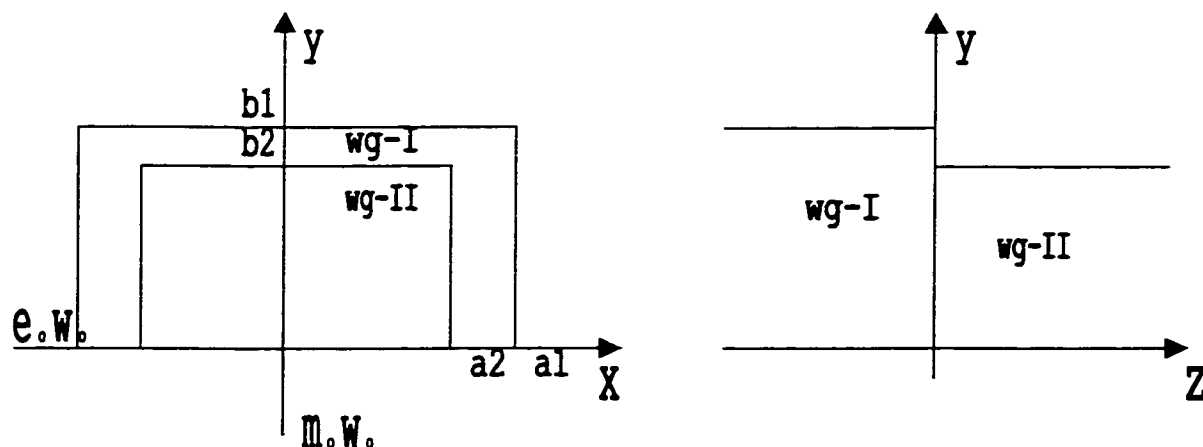
Figure 3.2.1 - Symmetrical Rectangular-to-Rectangular Waveguide Step

Symmetry planes are often used in electromagnetic numerical methods to reduce the mathematical complexity of the problem, which often translates into less computational effort. Because the two waveguides in figure 3.2.1 are symmetrically positioned about the origin, an artificial electric wall can be placed along the xz-plane and an artificial magnetic wall can be placed along the yz-plane without perturbing the electromagnetic fields inside the waveguides. A magnetic wall can be placed when it is known that the magnetic field lines are perpendicular to the magnetic wall surface and, therefore, only the transverse electric field lines are present there. Similarly, an electric wall can be placed when it is known that the electric field lines are perpendicular to the electric wall surface and, therefore, only the magnetic field lines are present there. By using these two symmetric planes, only one quarter of the discontinuity is considered during the analysis and the first quadrant, x > 0 and y > 0, will be considered in this thesis.

For the two rectangular waveguides shown in figure 3.2.1, the total electric and

magnetic fields inside each waveguide section can be expressed by the superposition of

the TE (or H) and TM (or E) wave components:

$$\bar{E}^v = \bar{E}^v_{TM} + \bar{E}^v_{TE} = \frac{1}{j\omega\varepsilon_o} \nabla \times \nabla \times (A^v_{Ez}\bar{e}_z) + \nabla \times (A^v_{Hz}\bar{e}_z)$$ (3.2.1)

$$\bar{H}^v = \bar{H}^v_{TE} + \bar{H}^v_{TM} = \frac{-1}{j\omega\mu_o} \nabla \times \nabla \times (A^v_{Hz}\bar{e}_z) + \nabla \times (A^v_{Ez}\bar{e}_z)$$ (3.2.2)

Expanding (3.2.1) and (3.2.2) show that the six field components are present inside

waveguide v and they can be derived from the z-directed Hertzian vector potentials

components, A_{Hz} and A_{Ez},

$$E^v_x = E^v_{xTM} + E^v_{xTE} = \frac{1}{j\omega\varepsilon_o} \frac{\partial^2 A^v_{Ez}}{\partial x \partial z} + \frac{\partial A^v_{Hz}}{\partial y}$$ (3.2.3a)

$$E^v_y = E^v_{yTM} + E^v_{yTE} = \frac{1}{j\omega\varepsilon_o} \frac{\partial^2 A^v_{Ez}}{\partial y \partial z} - \frac{\partial A^v_{Hz}}{\partial x}$$ (3.2.3b)

$$E^v_z = E^v_{zTM} + 0 = \frac{(k^v_{cEp})^2}{j\omega\varepsilon_o} A^v_{Ez}$$ (3.2.3c)

$$H^v_x = H^v_{xTE} + H^v_{xTM} = \frac{-1}{j\omega\mu_o} \frac{\partial^2 A^v_{Hz}}{\partial x \partial z} + \frac{\partial A^v_{Ez}}{\partial y}$$ (3.2.3d)

$$H^v_y = H^v_{yTE} + H^v_{yTM} = \frac{-1}{j\omega\mu_o} \frac{\partial^2 A^v_{Hz}}{\partial y \partial z} - \frac{\partial A^v_{Ez}}{\partial x}$$ (3.2.3e)

$$H^v_z = H^v_{zTE} + 0 = \frac{-(k^v_{cHq})^2}{j\omega\mu_o} A^v_{Hz}$$ (3.2.3f)

The Hertzian vector potentials are often used in electromagnetic boundary-value problems to represent the electric and magnetic fields. The advantage of using these vector potentials is that it simplifies the mathematical solution. For the rectangular waveguide v, the z-directed electric and magnetic vector potentials components, A_{Hz} and A_{Ez}, are defined by the superposition of all the TE and TM modes by

$$A_{Hz}^v = \sum_{m=0}^{\infty} \sum_{n=0}^{\infty} \sqrt{Z_{Hmn}^v}\, T_{Hmn}^v(x,y)\left(F_{Hmn}^v e^{-jk_{zHmn}^v z} + B_{Hmn}^v e^{+jk_{zHmn}^v z}\right) \tag{3.2.4}$$

$$A_{Ez}^v = \sum_{m=1}^{\infty} \sum_{n=1}^{\infty} \sqrt{Y_{Emn}^v}\, T_{Emn}^v(x,y)\left(F_{Emn}^v e^{-jk_{zEmn}^v z} - B_{Emn}^v e^{+jk_{zEmn}^v z}\right) \tag{3.2.5}$$

where the TE and TM wave impedances, wave admittances, and propagation constants are given by

$$Z_{Hmn}^v = \frac{\omega \mu_o}{k_{zHmn}^v} = \frac{1}{Y_{Hmn}^v} \tag{3.2.6}$$

$$Y_{Emn}^v = \frac{\omega \varepsilon_o}{k_{zEmn}^v} = \frac{1}{Z_{Emn}^v} \tag{3.2.7}$$

$$k_{zHmn}^v = \sqrt{k_o^2 - \left(k_{cHmn}^v\right)^2} \tag{3.2.8}$$

$$k_{zEmn}^v = \sqrt{k_o^2 - \left(k_{cEmn}^v\right)^2} \tag{3.2.9}$$

The F and B terms in equation (3.2.4) and (3.2.5) stand for the unknown forward and backward amplitude coefficients respectively. These are the coefficients that must be solved by matching the tangential fields at the discontinuity. In (3.2.8) and (3.2.9), k_{cHmn} and k_{cEmn} represent the TE_{mn} and TM_{mn} cut-off wave numbers or eigenvalues of the rectangular waveguide. Similarly, in (3.2.4) and (3.2.5), $T_{Hmn}(x,y)$ and $T_{Emn}(x,y)$ are the TE_{mn} and TM_{mn} wave functions or eigenfunctions of the rectangular waveguide. These wave numbers and wave functions are found by solving the wave equation for the transverse scalar potential wave functions $T_{Hmn}(x,y)$ and $T_{Emn}(x,y)$ given by

$$\left(\frac{d^2}{dx^2} + \frac{d^2}{dy^2} + k_{cM}^2 \right) T_M(x,y) = 0 \tag{3.2.10}$$

and applying the boundary conditions around the waveguide cross-section. Note that in (3.2.10), M is H or E depending if it is the transverse electric or magnetic wave respectively. For the rectangular waveguide cross-section shown in figure 3.2.1 with a magnetic wall at $x = 0$ and electric wall at $x = a_v$, $y = 0$ and $y = b_v$, the wave equation can easily be solved by the method of separation of variables leading to the following wave number and wave function solutions:

$$k_{cHmn}^v = \sqrt{\left(\frac{(2m-1)\pi}{2a_v} \right)^2 + \left(\frac{n\pi}{b_v} \right)^2} \tag{3.2.11}$$

$$k_{cEmn}^v = \sqrt{\left(\frac{(2m-1)\pi}{2a_v} \right)^2 + \left(\frac{n\pi}{b_v} \right)^2} \tag{3.2.12}$$

$$T_{Hmn}^{v}(x,y) = G_{Hmn}^{v} \frac{sin\left(\frac{(2m-1)\pi}{2a_v}x\right)cos\left(\frac{n\pi}{b_v}y\right)}{\sqrt{1+\delta_{0n}}}$$

(3.2.13)

(3.2.14)

$$T_{Emn}^{v}(x,y) = G_{Emn}^{v} cos\left(\frac{(2m-1)\pi}{2a_v}x\right)sin\left(\frac{n\pi}{b_v}y\right)$$

where δ_{0n} is the Kronecker delta function. The possible wave modes for the TE_{mn} waves are m = 1,2,3... and n = 0,1,2... whereas for the TM_{mn} waves m = 1,2,3... and n = 1,2,3.... The G_{Hmn} and G_{Emn} are normalizing wave coefficients, which limits the average power that each mode can carry to one Watt. The normalizing wave coefficients can be found by solving

$$P_{M}^{v} = \frac{1}{2}Re\left\{\int_{S}\left(\bar{E}_{M}^{v} \times \bar{H}_{M}^{v*}\right)\cdot d\bar{S}\right\} = 1$$

(3.2.15)

where M = H or E. For the rectangular cross-section shown in figure 3.2.1, the normalizing terms are given by,

$$G_{Hmn}^{v} = \frac{2\sqrt{2}}{k_{cHmn}^{v}\sqrt{a_v b_v}}$$

(3.2.16)

$$G_{Emn}^{v} = \frac{2\sqrt{2}}{k_{cEmn}^{v}\sqrt{a_v b_v}}$$

(3.2.17)

Now that the electromagnetic fields are totally described by equation (3.2.1) to (3.2.17) in wg-I and wg-II, the unknown forward and backward amplitude coefficients in equations (3.2.4) and (3.2.5) can be solved by matching the transverse field components E_x, E_y, H_x and H_y at the discontinuity. By matching the transverse electric field of wg-I on the left side with the transverse electric field of wg-II on the right side at $z = 0$, we obtain:

$$\sum_{q=1}^{\infty} \sqrt{Z_{Hq}^{I}}\left(\nabla T_{Hq}^{I} \times \vec{e}_z\right)\left(F_{Hq}^{I} + B_{Hq}^{I}\right) - \sum_{p=1}^{\infty} \sqrt{Z_{Ep}^{I}}\left(\nabla T_{Ep}^{I}\right)\left(F_{Ep}^{I} + B_{Ep}^{I}\right)$$

$$= \sum_{l=1}^{\infty} \sqrt{Z_{Hl}^{II}}\left(\nabla T_{Hl}^{II} \times \vec{e}_z\right)\left(F_{Hl}^{II} + B_{Hl}^{II}\right) - \sum_{k=1}^{\infty} \sqrt{Z_{Ek}^{II}}\left(\nabla T_{Ek}^{II}\right)\left(F_{Ek}^{II} + B_{Ek}^{II}\right)$$

(3.2.18)

where each indices q, p, k and l are related to the waveguide modes m, n by rearranging them with respect to increasing cut-off frequencies order. This transformation simplifies the analysis since it reduces the number of summation terms. Doing the same procedure for the tangential magnetic fields, we get:

$$\sum_{q=1}^{\infty} \sqrt{Y_{Hq}^{I}}\left(\nabla T_{Hq}^{I}\right)\left(F_{Hq}^{I} - B_{Hq}^{I}\right) + \sum_{p=1}^{\infty} \sqrt{Y_{Ep}^{I}}\left(\nabla T_{Ep}^{I} \times \vec{e}_z\right)\left(F_{Ep}^{I} - B_{Ep}^{I}\right)$$

$$= \sum_{l=1}^{\infty} \sqrt{Y_{Hl}^{II}}\left(\nabla T_{Hl}^{II}\right)\left(F_{Hl}^{II} - B_{Hl}^{II}\right) + \sum_{k=1}^{\infty} \sqrt{Y_{Ek}^{II}}\left(\nabla T_{Ek}^{II} \times \vec{e}_z\right)\left(F_{Ek}^{II} - B_{Ek}^{II}\right)$$

(3.2.19)

In order to eliminate the x and y dependence of the cross-section wave functions in (3.2.18) and (3.2.19), equation (3.2.18) is successively multiplied on both sides by $(\nabla T'_{Hq} \times e_z)$ and $(-\nabla T'_{Ep})$ and then integrated over the cross-section on both sides. Similarly, equation (3.2.19) is successively multiplied on both sides by $(\nabla T''_{Hl})$ and

$(\nabla T''_{Ek} \times \vec{e}_z)$ and then integrated over the cross-section on both sides. Using the orthogonality principals:

$$\int_{A^v} (\nabla T^v_{H,Er} \times \vec{e}_z)(\nabla T^v_{H,Es} \times \vec{e}_z)dA = \int_{A^v} (\nabla T^v_{H,Er})(\nabla T^v_{H,Es})dA = \delta_{rs} \qquad (3.2.20)$$

and

$$\int_{A^v} (\nabla T^v_{Er})(\nabla T^v_{Hs} \times \vec{e}_z)dA = \int_{A^v} (\nabla T^v_{Er} \times \vec{e}_z)(\nabla T^v_{Hs})dA \equiv 0 \qquad (3.2.21)$$

the four equations obtained can be simplified to

$$diag\left\{\sqrt{Z^I_{Hq}}\right\}(F^I_H + B^I_H) = \mathbf{J}_{HH} diag\left\{\sqrt{Z^{II}_{Hl}}\right\}(F^{II}_H + B^{II}_H) \qquad (3.2.22)$$

$$diag\left\{\sqrt{Z^I_{Ep}}\right\}(F^I_E + B^I_E) = \mathbf{J}_{EH} diag\left\{\sqrt{Z^{II}_{Hl}}\right\}(F^{II}_H + B^{II}_H) + \mathbf{J}_{EE} diag\left\{\sqrt{Z^{II}_{Ek}}\right\}(F^{II}_E + B^{II}_E) \qquad (3.2.23)$$

$$\mathbf{J}^T_{HH} diag\left\{\sqrt{Y^I_{Hq}}\right\}(F^I_H - B^I_H) + \mathbf{J}^T_{EH} diag\left\{\sqrt{Y^I_{Ep}}\right\}(F^I_E - B^I_E) = diag\left\{\sqrt{Y^{II}_{Hl}}\right\}(F^{II}_H - B^{II}_H) \qquad (3.2.24)$$

$$\mathbf{J}^T_{EE} diag\left\{\sqrt{Y^I_{Ep}}\right\}(F^I_E - B^I_E) = diag\left\{\sqrt{Y^{II}_{Ek}}\right\}(F^{II}_E - B^{II}_E) \qquad (3.2.25)$$

where the infinite series in (3.2.18) and (3.2.19) can be truncated to P, Q, L and K terms to yield the matrix equations (3.2.22) to (3.2.25). The superscript, T, means that the matrix is transposed. The matrices, $\mathbf{J}$, are called the coupling matrices. The four coupling matrices are defined by

$$\left(\mathbf{J}_{HH}\right)_{ql} = \int_{A^{II}}\left(\nabla T_{Hq}^{I} \times \vec{e}_{z}\right)\left(\nabla T_{Hl}^{II} \times \vec{e}_{z}\right)dA \tag{3.2.26}$$

$$\left(\mathbf{J}_{EH}\right)_{pl} = \int_{A^{II}}\left(-\nabla T_{Ep}^{I}\right)\left(\nabla T_{Hl}^{II} \times \vec{e}_{z}\right)dA \tag{3.2.27}$$

$$\left(\mathbf{J}_{EE}\right)_{pk} = \int_{A^{II}}\left(\nabla T_{Ep}^{I}\right)\left(\nabla T_{Ek}^{II}\right)dA \tag{3.2.28}$$

$$\left(\mathbf{J}_{HE}\right)_{qk} = \int_{A^{II}}\left(\nabla T_{Hq}^{I} \times \vec{e}_{z}\right)\left(\nabla T_{Ek}^{II}\right)dA \tag{3.2.29}$$

Isolating for the forward and backward wave amplitude coefficients in (3.2.22) to (3.2.25) yields the modal scattering matrix of the step discontinuity shown in figure 3.2.1,

$$\mathbf{S}_{11} = -\mathbf{W}(\mathbf{U} - \mathbf{M}\mathbf{M}^{T}) \tag{3.2.30}$$

$$\mathbf{S}_{12} = 2\mathbf{W}\mathbf{M} \tag{3.2.31}$$

$$\mathbf{S}_{21} = \mathbf{M}^{T}\left\{\mathbf{U} + \mathbf{W}(\mathbf{U} - \mathbf{M}\mathbf{M}^{T})\right\} = \mathbf{M}^{T}\left\{\mathbf{U} - \mathbf{S}_{11}\right\} \tag{3.2.32}$$

$$\mathbf{S}_{22} = \mathbf{U} - 2\mathbf{M}^{T}\mathbf{W}\mathbf{M} = \mathbf{U} - \mathbf{M}^{T}\mathbf{S}_{12} \tag{3.2.33}$$

where U is the unity matrix and, W is given by

$$\mathbf{W} = (\mathbf{U} + \mathbf{M}\mathbf{M}^{T})^{-1} \tag{3.2.34}$$

where

$$
\mathbf{M} = \begin{bmatrix} diag\left\{\sqrt{Y_{Hq}^{I}}\right\}\mathbf{J}_{HH}diag\left\{\sqrt{Z_{Hl}^{II}}\right\} & diag\left\{\sqrt{Y_{Hq}^{I}}\right\}\mathbf{J}_{HE}diag\left\{\sqrt{Z_{Ek}^{II}}\right\} \\ diag\left\{\sqrt{Y_{Ep}^{I}}\right\}\mathbf{J}_{EH}diag\left\{\sqrt{Z_{Hl}^{II}}\right\} & diag\left\{\sqrt{Y_{Ep}^{I}}\right\}\mathbf{J}_{EE}diag\left\{\sqrt{Z_{Ek}^{II}}\right\} \end{bmatrix} \qquad (3.2.35)
$$

The S-parameters in (3.2.30) to (3.2.33) is the MM solution to the symmetrical rectangular-to-rectangular waveguide step shown in figure 3.2.1. It includes the reflection and transmission coefficients related to the fundamental mode as well as the higher-order modes and, for this reason, it is called the generalized scattering matrix (GSM). For example, the matrix element, $S_{21}(p,q)$, represents the transmission coefficient of the pth wave mode in wg-II if the qth wave mode is incident in wg-I. In the next section, the symmetrical rectangular-to-ridge waveguide step will be solved.

3.3   Symmetrical Rectangular-to-Ridged Waveguide Step

The second discontinuity that will be analyzed by the MMM in this thesis is the symmetrical rectangular-to-ridge waveguide step shown in figure 3.3.1. Two waveguides are involved in this discontinuity, namely the rectangular waveguide and the ridged waveguide. Again, the two waveguides are symmetrically positioned about the origin so that symmetry planes can be used to simplify the analysis.
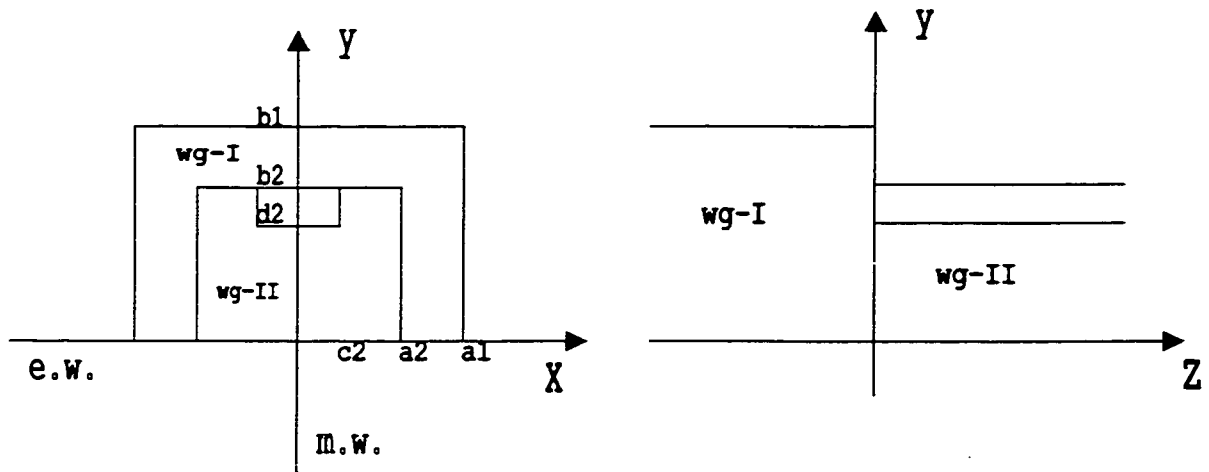
Figure 3.3.1 - Symmetrical Rectangular-to-Ridged Waveguide Step

For the rectangular waveguide, wg-I, the wave numbers and wave functions, (3.2.11) to (3.2.14), were obtained by solving the wave equation for the bounded rectangular cross-section using the separation of variable method. Using equations (3.2.11) to (3.2.14), the electromagnetic fields inside the rectangular waveguide are fully described by equations (3.2.1) to (3.2.5).

For the ridged waveguide, wg-II, the wave numbers and wave functions need to be solved so that the total electromagnetic fields inside wg-II is fully described by equations (3.2.1) to (3.2.5). Because of the fin inside the guide, the wave equation cannot be evaluated exactly for such geometrical bounded problem. Therefore, the wave numbers and functions must be evaluated numerically.

Because the ridged waveguide is often used in microwave structures, some numerical methods [19-21] have been published to solve wave equation for the ridged waveguide geometry. The Ritz-Galerkin method is used in [19] to solve the TE and TM wave numbers and functions of the ridged waveguide. In [20] a variational approach is used. In [21], three different methods are presented and compared.

In this section the following approach will be used for the symmetrical ridged waveguide cross-section shown in figure 3.3.2. The ridged waveguide will be divided into two rectangular subsections, II-a and II-b. Imposing the electric and magnetic walls in each subregion, the wave functions in each subregions will be derived. Finally, the transverse fields will be matched at the interface of the two subregions to yield the wave numbers and functions of the symmetrical ridged waveguide. Like in the separation of variables method used to find the wave numbers and functions of the rectangular waveguide, this approach will have to be done twice: once for the TE waves and once for the TM waves.
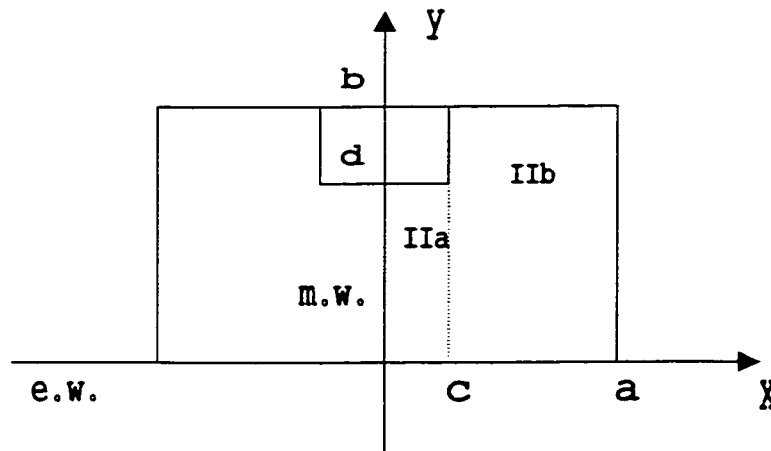
Figure 3.3.2 - Symmetrical Ridged Waveguide Cross-Section

Ridged Waveguide TE Waves

First, the wave equation (3.2.10) needs to be solved for $T_H(x,y)$ in region IIa and

IIb. The boundary conditions in region IIa are a magnetic wall at $x = 0$ and electric walls

at $y = 0$ and d, whereas region IIb has only electric walls at $x = a$, $y = 0$ and b. From the

general solution to the wave equation in each region and imposing the boundary

conditions, the tranverse scalar potential functions may be expanded as the sum of

weighted mode functions by

$$(3.3.1)$$

$$T_{Hr}^{II}(x,y) = \begin{cases} G_{Hr}^{II} \sum_{m=0}^{M} A_{Hrm}^{IIa} \sin(k_{xHrm}^{IIa} x) \dfrac{\cos\left(\dfrac{m\pi}{d}y\right)}{\sqrt{1+\delta_{0m}}} & ,0 \leq x \leq c \wedge 0 \leq y \leq d \\ \\ G_{Hr}^{II} \sum_{n=0}^{N} A_{Hrn}^{IIb} \cos(k_{xHrn}^{IIb}(a-x)) \dfrac{\cos\left(\dfrac{n\pi}{b}y\right)}{\sqrt{1+\delta_{0n}}} & ,c \leq x \leq a \wedge 0 \leq y \leq b \end{cases}$$

where M terms are used in region IIa and N terms are used in region IIb. The x-

component wave numbers, k_{xH}, are given by

$$k_{xHrm}^{IIa} = \sqrt{k_{cHr}^{II}{}^2 - \left(\frac{m\pi}{d}\right)^2} \qquad (3.3.2)$$

$$k_{xHrn}^{IIb} = \sqrt{k_{cHr}^{II}{}^2 - \left(\frac{n\pi}{b}\right)^2} \qquad (3.3.3)$$

The y-directed electric fields, E_y, and the z-directed magnetic fields, H_z, of region IIa and IIb are then matched at x = c. Using (3.2.3b), (3.2.3f) and (3.3.1), we get:

$$\sum_{n=0}^{N} A_{Hrn}^{IIb} k_{xHrn}^{IIb} sin\left(k_{xHrn}^{IIb}(a-c)\right)\frac{cos\left(\dfrac{n\pi}{b}y\right)}{\sqrt{1+\delta_{0n}}} = \sum_{m=0}^{M} A_{Hrm}^{IIa} k_{xHrm}^{IIa} cos\left(k_{xHrm}^{IIa}c\right)\frac{cos\left(\dfrac{m\pi}{d}y\right)}{\sqrt{1+\delta_{0m}}} \qquad (3.3.4)$$

$$\sum_{n=0}^{N} A_{Hrn}^{IIb} cos\left(k_{xHrn}^{IIb}(a-c)\right)\frac{cos\left(\dfrac{n\pi}{b}y\right)}{\sqrt{1+\delta_{0n}}} = \sum_{m=0}^{M} A_{Hrm}^{IIa} sin\left(k_{xHrm}^{IIa}c\right)\frac{cos\left(\dfrac{m\pi}{d}y\right)}{\sqrt{1+\delta_{0m}}} \qquad (3.3.5)$$

In order to eliminate the y dependence in (3.3.4), we need to multiply both sides of (3.3.4) by $cos(n\pi y/b)/sqrt(1+\delta_{0n})$ and integrate both sides from y = 0 to b. Similarly, we can multiply both sides of (3.3.5) by $cos(m\pi y/d)/sqrt(1+\delta_{0m})$ and integrate both sides from y = 0 to d.

$$(3.3.6)$$

$$A_{Hrn}^{IIb} k_{xHrn}^{IIb} sin\left(k_{xHrn}^{IIb}(a-c)\right)\frac{b}{2} = \sum_{m=0}^{M} A_{Hrm}^{IIa} k_{xHrm}^{IIa} cos\left(k_{xHrm}^{IIa}c\right)\int_{0}^{d} \frac{cos\left(\dfrac{m\pi}{d}y\right)}{\sqrt{1+\delta_{0m}}}\frac{cos\left(\dfrac{n\pi}{b}y\right)}{\sqrt{1+\delta_{0n}}}dy$$

$$\sum_{n=0}^{N} A_{Hrn}^{IIb} cos\left(k_{xHrn}^{IIb}(a-c)\right)\int_{0}^{d} \frac{cos\left(\dfrac{m\pi}{d}y\right)}{\sqrt{1+\delta_{0m}}}\frac{cos\left(\dfrac{n\pi}{b}y\right)}{\sqrt{1+\delta_{0n}}}dy = A_{Hrm}^{IIa} sin\left(k_{xHrm}^{IIa}c\right)\frac{d}{2} \qquad (3.3.7)$$

Equation (3.3.6) and (3.3.7) can be simplified to the following system of linear equations:

$$A_{Hrn}^{IIb} = [LE]_{nm} A_{Hrm}^{IIa} \tag{3.3.8}$$

$$[LH]_{mn} A_{Hrn}^{IIb} = A_{Hrm}^{IIa} \tag{3.3.9}$$

where the *LE* and the *LH* matrices are given by

$$[LE]_{nm} = \frac{2\, k_{xHrm}^{IIa} \cos\left(k_{xHrm}^{IIa} c\right)}{b\, k_{xHrn}^{IIb} \sin\left(k_{xHrn}^{IIb}(a-c)\right)} I(m,n) \tag{3.3.10}$$

$$[LH]_{mn} = \frac{2\, \cos\left(k_{xHrn}^{IIb}(a-c)\right)}{d\, \sin\left(k_{xHrm}^{IIa} c\right)} I(m,n) \tag{3.3.11}$$

where I(m,n) is the solution of the integral in (3.3.6) and (3.3.7), given by

$$\tag{3.3.12}$$

$$I(m,n) = \begin{cases} \dfrac{d}{2} + \dfrac{\sin\left(\dfrac{2m\pi}{d}\right)}{\dfrac{4m\pi}{d}} & , \dfrac{m\pi}{d} = \dfrac{n\pi}{b} \\[4ex] \dfrac{1}{\sqrt{1+\delta_{0m}}}\dfrac{1}{\sqrt{1+\delta_{0n}}}\left[\dfrac{\sin\left(\left(\dfrac{m\pi}{d}-\dfrac{n\pi}{b}\right)d\right)}{2\left(\dfrac{m\pi}{d}-\dfrac{n\pi}{b}\right)} + \dfrac{\sin\left(\left(\dfrac{m\pi}{d}+\dfrac{n\pi}{b}\right)d\right)}{2\left(\dfrac{m\pi}{d}+\dfrac{n\pi}{b}\right)} \right] & , otherwise \end{cases}$$

By substituting (3.3.8) into (3.3.9), we obtain a system of homogeneous linear equations, Q, in terms of the amplitude coefficients of the wave functions in region IIa, A^{IIa},

$$\begin{bmatrix} Q_{00} & Q_{01} & \cdots & Q_{0M} \\ Q_{10} & Q_{11} & \cdots & Q_{1M} \\ \vdots & \vdots & \ddots & \vdots \\ Q_{M0} & Q_{M1} & \cdots & Q_{MM} \end{bmatrix} \begin{bmatrix} A_{Hr0}^{IIa} \\ A_{Hr1}^{IIa} \\ \vdots \\ A_{HrM}^{IIa} \end{bmatrix} = \begin{bmatrix} 0 \\ 0 \\ \vdots \\ 0 \end{bmatrix}$$

(3.3.13)

where

$$\left[Q\left(k_{cHr}^{II} \right) \right]_{mm} = U_{mn} - [LH]_{mn} [LE]_{nm}$$

(3.3.14)

Note that (3.3.14) is a function of the cutoff wave number of the ridged waveguide. In order to solve for the TE modes, we need to find the cutoff wave numbers, k_{cH}, such that the determinant of matrix Q is zero. This can mathematically be written as

$$k_{cHr}^{II} = \left\{ k_{cHr}^{II} \middle| \det\left(\left[Q\left(k_{cHr}^{II} \right) \right]_{mm} \right) = 0 \right\}$$

(3.3.15)

When a wave number, k_{cH}, is found, the amplitude coefficients A^{IIa} and A^{IIb} in (3.3.1) for this waveguide mode. These coefficients can be computed by substituting

$$A_{Hr0}^{IIa} = 1$$

in (3.3.13) and rearranging (3.3.13), we get an overdetermined system of M unknowns and $M+1$ equations as follows:

$$
\begin{bmatrix}
Q_{01} & Q_{02} & \cdots & Q_{0M} \\
Q_{11} & Q_{12} & \cdots & Q_{1M} \\
\vdots & \vdots & \ddots & \vdots \\
Q_{M1} & Q_{M2} & \cdots & Q_{MM}
\end{bmatrix}
\begin{bmatrix}
A_{Hr1}^{IIa} \\
A_{Hr2}^{IIa} \\
\vdots \\
A_{HrM}^{IIa}
\end{bmatrix}
=
\begin{bmatrix}
-Q_{00} \\
-Q_{10} \\
\vdots \\
-Q_{M0}
\end{bmatrix}
\tag{3.3.16}
$$

This system of equations can now be solved numerically in the least square sense for the remaining amplitude coefficients A^{IIa}. Once all the A^{IIa} are known, the A^{IIb} coefficients can be solved using (3.3.8). When all the wave numbers and wave function coefficients are known, the normalization coefficients in (3.3.1), G^{II}, need to be solved so that each TE mode can carry a maximum of one Watt. Using (3.2.15), we find that

$$
P_{Hr}^{II} = \frac{1}{2} G_{Hr}^{II\,2}
\left\{
\begin{aligned}
& \sum_{m=0}^{M} A_{Hrm}^{IIa\,2} k_{xHrm}^{IIa\,2} \left(\frac{c}{2} + \frac{sin\left(2k_{xHrm}^{IIa}c\right)}{4k_{xHrm}^{IIa}} \right) \frac{d}{2} \\
& + \sum_{m=0}^{M} A_{Hrm}^{IIa\,2} \left(\frac{m\pi}{d} \right)^2 \left(\frac{c}{2} - \frac{sin\left(2k_{xHrm}^{IIa}c\right)}{4k_{xHrm}^{IIa}} \right) \frac{d}{2} \\
& + \sum_{n=0}^{N} A_{Hrn}^{IIb\,2} k_{xHrn}^{IIb\,2} \left(\frac{(a-c)}{2} - \frac{sin\left(2k_{xHrn}^{IIb}(a-c)\right)}{4k_{xHrn}^{IIb}} \right) \frac{b}{2} \\
& + \sum_{n=0}^{N} A_{Hrn}^{IIb\,2} \left(\frac{n\pi}{b} \right)^2 \left(\frac{(a-c)}{2} + \frac{sin\left(2k_{xHrn}^{IIb}(a-c)\right)}{4k_{xHrn}^{IIb}} \right) \frac{b}{2}
\end{aligned}
\right\} = 1
\tag{3.3.17}
$$

This completes the analysis to find the TE wave numbers and wave functions of the ridged waveguide shown in figure 3.3.2. The same analysis needs to be done, but this time for the TM waves.

Ridged Waveguide TM Waves

Since the procedure to obtain the ridged waveguide TM modes is very similar to the TE modes, only the main steps will be discussed here. Again, the wave equation (3.2.10) needs to be solved for the TM transverse potential functions, $T_E(x,y)$, in region IIa and IIb. The boundary conditions in region IIa are still a magnetic wall at $x = 0$ and an electric walls at $y = 0$ and d, whereas region IIb only has electric walls at $x = a$, $y = 0$ and b. However, since we are dealing with TM waves, the cross-section functions are now expanded as

$$(3.3.18)$$

$$T_{Es}^{II}(x,y) = \begin{cases} G_{Es}^{II} \sum_{m=1}^{M} A_{Esm}^{IIa} \cos(k_{xEsm}^{IIa} x) \sin\left(\frac{m\pi}{d} y\right) & ,0 \leq x \leq c \wedge 0 \leq y \leq d \\ G_{Es}^{II} \sum_{n=1}^{N} A_{Esn}^{IIb} \sin(k_{xHrn}^{IIb}(a-x)) \sin\left(\frac{n\pi}{b} y\right) & ,c \leq x \leq a \wedge 0 \leq y \leq b \end{cases}$$

where

$$k_{xEsm}^{IIa} = \sqrt{k_{cEs}^{II\ 2} - \left(\frac{m\pi}{d}\right)^2} \qquad\qquad (3.3.19)$$

$$k_{xEsn}^{IIb} = \sqrt{k_{cEs}^{II\ 2} - \left(\frac{n\pi}{b}\right)^2} \qquad\qquad (3.3.20)$$

By matching the z-directed electric fields, E_z, and y-directed magnetic fields, H_y, at the

interface of region IIa and IIb, we obtain the following system of linear equations:

$$A_{Esn}^{IIb} = \left[LE \right]_{nm} A_{Esm}^{IIa} \tag{3.3.21}$$

$$\left[LH \right]_{mn} A_{Esn}^{IIb} = A_{Esm}^{IIa} \tag{3.3.22}$$

where

$$\left[LE \right]_{nm} = \frac{2 \cos\left(k_{xEsm}^{IIa} c \right)}{b \sin\left(k_{xEsn}^{IIb} (a - c) \right)} I(m,n) \tag{3.3.23}$$

$$\left[LH \right]_{mn} = \frac{2 \, k_{xEsn}^{IIb} \cos\left(k_{xEsn}^{IIb} (a - c) \right)}{d \, k_{xEsm}^{IIa} \sin\left(k_{xEsm}^{IIa} c \right)} I(m,n) \tag{3.3.24}$$

and $I(m,n)$ is given by (3.3.12). Substituting (3.3.21) into (3.3.22) leads to a system of

equations,

$$\begin{bmatrix} Q_{11} & Q_{12} & \cdots & Q_{1M} \\ Q_{21} & Q_{22} & \cdots & Q_{2M} \\ \vdots & \vdots & \ddots & \vdots \\ Q_{M1} & Q_{M2} & \cdots & Q_{MM} \end{bmatrix} \begin{bmatrix} A_{Es1}^{IIa} \\ A_{Es2}^{IIa} \\ \vdots \\ A_{EsM}^{IIa} \end{bmatrix} = \begin{bmatrix} 0 \\ 0 \\ \vdots \\ 0 \end{bmatrix} \tag{3.3.25}$$

where

$$\left[Q\left(k''_{cEs}\right)\right]_{mm} = U_{mm} - \left[LH\right]_{mn}\left[LE\right]_{nm} \qquad (3.3.26)$$

Equation (3.3.26) can be solved for the TM eigenvalues of the ridged waveguide as follows:

$$k''_{cEs} = \left\{ k''_{cEs} \mid \det\left(\left[Q\left(k''_{cEs}\right)\right]_{mm}\right) = 0 \right\} \qquad (3.3.27)$$

Once a wave number is found, the corresponding wave functions amplitude coefficients for the same mode must be computed by the same method discussed in section 3.3.1. Finally, the normalization constant for each TM mode is given by

$$P''_{E,} = \frac{1}{2} G''^{2}_{Es} \left\{ \begin{array}{l} \sum\limits_{m=1}^{M} A^{IIa\,2}_{Esm} k^{IIa\,2}_{xEsm} \left(\dfrac{c}{2} - \dfrac{sin\left(2k^{IIa}_{xEsm}c\right)}{4k^{IIa}_{xEsm}} \right)\dfrac{d}{2} \\[3mm] + \sum\limits_{m=1}^{M} A^{IIa\,2}_{Esm} \left(\dfrac{m\pi}{d}\right)^{2}\left(\dfrac{c}{2} + \dfrac{sin\left(2k^{IIa}_{xEsm}c\right)}{4k^{IIa}_{xEsm}} \right)\dfrac{d}{2} \\[3mm] + \sum\limits_{n=1}^{N} A^{IIb\,2}_{Esn} k^{IIb\,2}_{xEsn} \left(\dfrac{(a-c)}{2} + \dfrac{sin\left(2k^{IIb}_{xEsn}(a-c)\right)}{4k^{IIb}_{xEsn}} \right)\dfrac{b}{2} \\[3mm] + \sum\limits_{n=1}^{N} A^{IIb\,2}_{Esn} \left(\dfrac{n\pi}{b}\right)^{2}\left(\dfrac{(a-c)}{2} - \dfrac{sin\left(2k^{IIb}_{xEsn}(a-c)\right)}{4k^{IIb}_{xEsn}} \right)\dfrac{b}{2} \end{array} \right\} = 1 \qquad (3.3.29)$$

Once that all the wave numbers and wave functions for all the TE and TM modes are computed for the rectangular waveguide and for the ridged waveguide, the same MMM derived in section 3.2 can be used to obtain the scattering matrix of the

rectangular-to-ridged waveguide step. However, this time the coupling matrices, (3.2.26)

to (3.2.29), increase complexity since the wave functions (3.3.1) and (3.3.18) must be

used for waveguide $v = II$.

Before proceeding to the next chapter, which will show how to cascade scattering

matrices to obtain fullwave analysis of microwave structures and components, the

accuracy of (3.3.15) to find the ridged waveguide wave numbers will be discussed.

Ridged Waveguide Modes Convergence

Table 3.3.1 shows the convergence for the three first TE wave numbers of a

symmetrical ridged waveguide with a = 0.250", b = 0.200", c = 0.050", and d = 0.055" as

a function of the number of terms used in the field expansions in region IIa, M, and

region IIb, N. The third, fifth and sixth column results were obtained using the equations

derived in section 3.3.1 whereas the fourth and seventh column results are from [19].

Comparing the wave numbers obtained by the method proposed in section 3.3.1 with

those in [19], it is shown that both methods exhibit convergence and good agreement.

Table 3.3.1 - Three First TE Modes For The Symmetrical Ridged Waveguide

M terms	N terms	kc-TE1 (rad/in) Section 3.3.1	kc-TE1 (rad/in) [19]	kc-TE2 (rad/in) Section 3.3.1	kc-TE3 (rad/in) Section 3.3.1	kc-TE2 (rad/in) [19]
1	1	3.7624	4.4257	15.7358	17.1373	---
1	5	3.6567	3.6475	15.7236	17.0503	17.0583
1	20	3.6441	3.6275	15.7229	17.0453	17.0454
5	5	3.6682	3.6911	15.7286	17.0517	17.0614
5	10	3.6602	3.6654	15.7274	17.0486	17.0514
5	20	3.6532	3.6520	15.7263	17.0466	17.0469
5	40	3.6518	3.6491	15.7261	17.0462	17.0459
5	60	3.6516	3.6486	15.7261	17.0461	17.0457
5	99	3.6515	3.6483	15.7261	17.0460	17.0457
10	10	3.6610	3.6682	15.7277	17.0487	17.0517
10	20	3.6558	3.6602	15.7269	17.0472	17.0486
10	60	3.6528	3.6522	15.7264	17.0463	17.0463
10	80	3.6526	3.6518	15.7264	17.0463	17.0462
10	99	3.6526	3.6517	15.7264	17.0463	17.0461

CHAPTER 4 – Generalized Scattering Matrix Method

In chapter three, MMM was use to extract the GSM at the junction of two dissimilar waveguides. The scattering matrix obtained is said generalized because it measures the fundamental mode and the higher-order modes scattering parameters. Because all the modes are included, when two or more GSMs are in cascade, the overall GSM obtained accurately predicts the scattering phenomena [4]. Therefore, a microwave circuit composed of various waveguide sections can be decomposed in terms of its GSMs. Then, the overall GSM of the circuit can be computed by the GSM method.

In this chapter, we will introduce the principles of the GSM method through two examples. Since the GSM method cannot be used alone and must be combined with another numerical method such as the MMM presented in the previous chapter, the convergence of the combined MM-GSM method will be discussed for each example.

4.1   Symmetrical Rectangular Waveguide Iris

A common waveguide structure that is often used in the construction of microwave couplers and filters is the symmetrical rectangular waveguide iris shown in figure 4.1.1. A larger rectangular waveguide, wg-I, is separated from another rectangular waveguide with the same cross-section by a smaller rectangular waveguide, wg-II, with a

finite length, L. Figure 4.1.1 also shows the forward, F, and backward, B, amplitude coefficients in each waveguide.
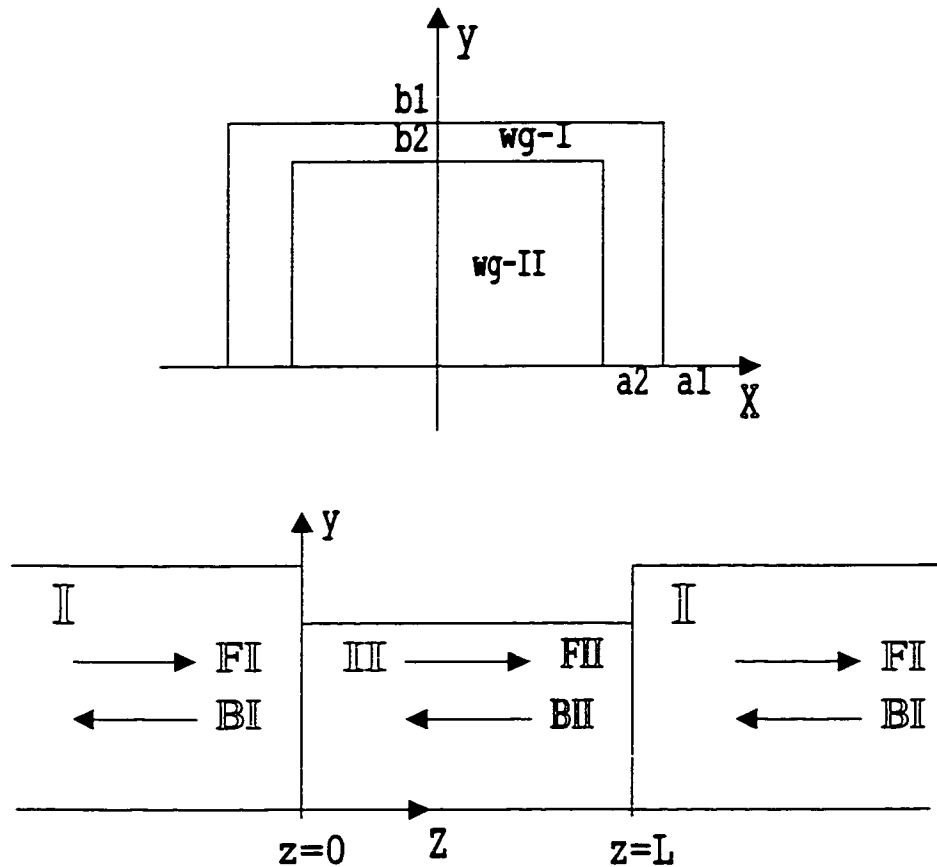
Figure 4.1.1 - Symmetrical Rectangular Waveguides Iris

The GSM method consists on concatenating all the GSMs to obtain the overall GSM of the microwave circuit. But, first, we need to determine all the discontinuities in the structure. In figure 4.1.1, two waveguide steps are encountered. The first waveguide step is created by the junction of wg-I with wg-II at z = 0. The second waveguide step is created by the junction of wg-II with wg-I at z = L. The second step in the procedure consists on solving the GSM for each discontinuity encountered. For the symmetrical

rectangular waveguide step between wg-I and wg-II, we can use the equations derived in

section 3.2 of this thesis. The GSM for the waveguide step at z = L can be obtained by

simply inverting the ports 1 and 2 for the GSM found at z = 0. For example, if the GSM

at z = 0 is defined by, SA:

$$SA = \begin{bmatrix} SA_{11} & SA_{12} \\ SA_{21} & SA_{22} \end{bmatrix}$$

(4.1.1)

then, the GSM at z = L is defined by, SB:

$$SB = \begin{bmatrix} SB_{11} & SB_{12} \\ SB_{21} & SB_{22} \end{bmatrix} = \begin{bmatrix} SA_{22} & SA_{21} \\ SA_{12} & SA_{11} \end{bmatrix}$$

(4.1.2)

The third step consists on defining the transmission GSM for each waveguide with finite

length. In this example, only wg-II has a finite length of L and the two wg-I are assumed

to be zero length. The transmission GSM for wg-II is given by, SC:

$$SC = \begin{bmatrix} 0 & D \\ D & 0 \end{bmatrix}$$

(4.1.3)

where the SC_{11} and SC_{22} submatrices in (4.1.3) are matrices with all its elements equal to

zero and D is a matrix defined by

$$D = \begin{bmatrix} diag\left(e^{-jk_{zH}^{II}L}\right) & 0 \\ 0 & diag\left(e^{-jk_{zE}^{II}L}\right) \end{bmatrix}$$

(4.1.4)

where the D_{12} and D_{21} submatrices in (4.1.4) are matrices with all its elements equal to zero and k^{II}_{zH} and k^{II}_{zE} are the TE and TM propagation wave propagation constants found in wg-II. Figure 4.1.2 shows the equivalent GSM representation to the rectangular waveguide iris shown in figure 4.1.1.

$$\boxed{\begin{matrix} SA_{11} & SA_{12} \\ SA_{21} & SA_{22} \end{matrix}} \quad \boxed{\begin{matrix} SC_{11} & SC_{12} \\ SC_{21} & SC_{22} \end{matrix}} \quad \boxed{\begin{matrix} SB_{11} & SB_{12} \\ SB_{21} & SB_{22} \end{matrix}}$$
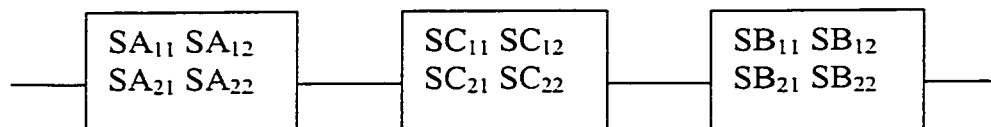
Figure 4.1.2 - Equivalent GSM Representation for the Rectangular Waveguide Iris

Finally, the last step consists of successively cascading the GSM until the overall GSM of the structure is obtained. For two two-port networks, the GSMs, SL and SR shown in figure 4.1.3, can be cascaded to obtain the equivalent GSM, ST,

$$\boxed{\begin{matrix} SL_{11} & SL_{12} \\ SL_{21} & SL_{22} \end{matrix}} \quad \boxed{\begin{matrix} SR_{11} & SR_{12} \\ SR_{21} & SR_{22} \end{matrix}}$$

$$\boxed{\begin{matrix} ST_{11} & ST_{12} \\ ST_{21} & ST_{22} \end{matrix}}$$

Figure 4.1.3 - Cascading two-port GSM

$$ST_{11} = SL_{11} + SL_{12}SR_{11}WSL_{12} \qquad (4.2.5a)$$

$$ST_{12} = SL_{12}(U + SR_{11}WSL_{22})SR_{12} \qquad (4.2.5b)$$

$$ST_{21} = SR_{21}WSL_{21} \qquad (4.2.5c)$$

$$ST_{22} = SR_{22} + SR_{21}WSL_{22}SR_{12} \qquad (4.2.5d)$$

where U is the unitary matrix and W is equal to

$$W = (U - SL_{22}SR_{11})^{-1} \qquad (4.2.6)$$

Therefore, the overall GSM of the rectangular waveguide iris is computed by, first, cascading SA with SC to obtain a new two port GSM and then, cascade this new GSM with SB.

Combining the MM and GSM methods, a computer program was written in Matlab to compute the S-parameters of a rectangular iris of finite length. Table 4.1.1 shows the convergence of the MM-GSM method for the three-dimensional iris structure shown in figure 4.1.1 with input and output waveguide ports using standard rectangul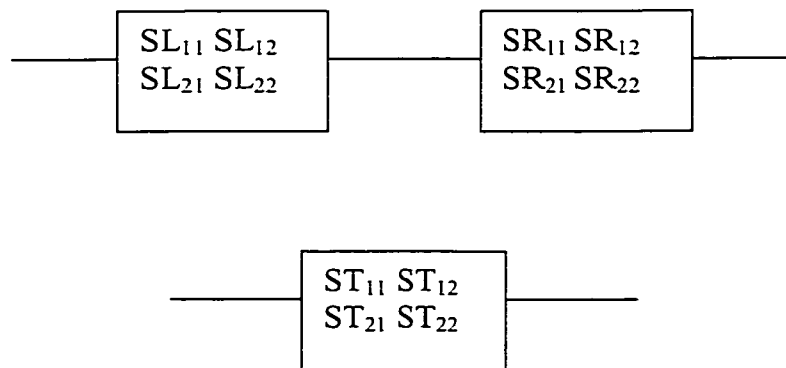ar waveguides WR75 ($a_1 = 0.375$" by $b_1 = 0.1875$"), the iris cross-section is $a_2 = 0.200$" by $b_2 = 0.100$", the thickness of the iris is $L = 0.100$", and the operational frequency is 10 GHz. Instead of randomly selecting the number of TE and TM modes in each waveguide, the number of modes is limited by given a maximal cut-off frequency (first column of table 4.1.1). As the maximal cut-off frequency is increased, more modes are used in the computation of the coupling matrices and the S-parameters converge to $|S_{11}| =$

0.9543 and $|S_{21}| = 0.2989$ after a maximal cutoff frequency of 100 GHz as illustrated by table 4.1.1 and figure 4.1.4.

Table 4.1.1 – S-Parameters Convergence for a Rectangular Waveguide Iris

f_{cutoff} GHz	wg-I modes TE – TM	wg-II modes TE – TM	$|S_{11}|$	$|S_{21}|$
20	1 – 0	1 – 0	0.8137	0.5813
25	2 – 0	1 – 0	0.9389	0.3442
35	3 – 1	1 – 0	0.9306	0.3660
40	5 – 2	1 – 0	0.9536	0.3010
55	6 – 3	2 – 0	0.9444	0.3287
61	7 – 3	3 – 1	0.9510	0.3092
70	10 - 6	3 – 1	0.9535	0.3015
90	15 – 9	5 – 2	0.9529	0.3033
100	19 – 13	6 – 3	0.9543	0.2988
125	28 – 20	9 – 5	0.9543	0.2988
150	40 – 30	13 – 8	0.9543	0.2989
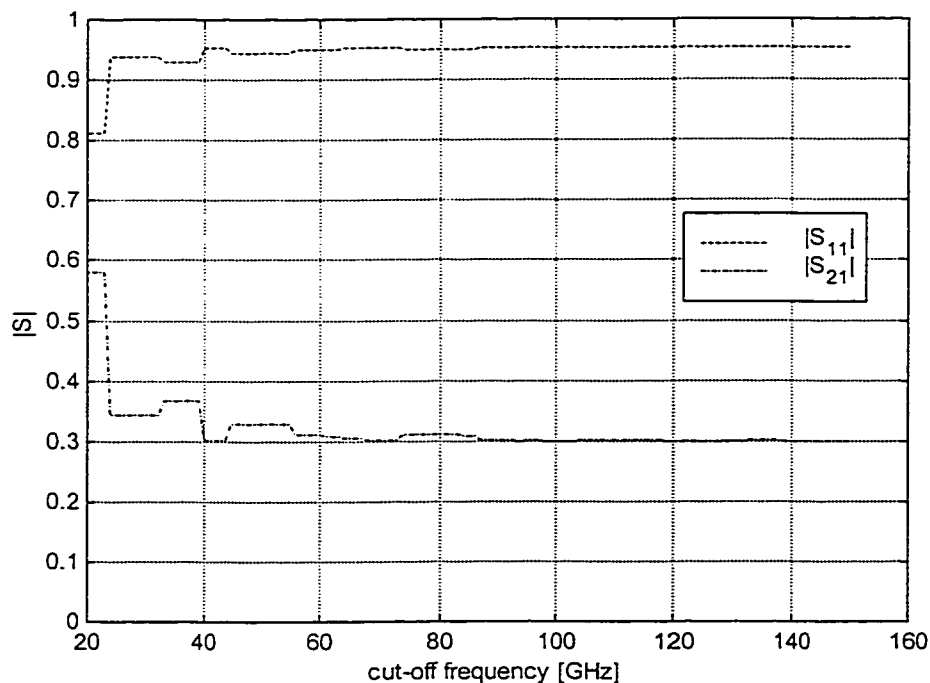
Figure 4.1.4 – S-Parameters Convergence for a Rectangular Waveguide Iris

4.2 Symmetrical Ridged Waveguide Coupling

In order to demonstrate the accuracy of the MM-GSM method to solve discontinuities involving rectangular-to-ridged waveguide steps, the structure shown in figure 4.2.1 will be solved. Figure 4.2.1 shows the symmetrical ridged waveguide coupling structure, which consists of two propagating ridged waveguides, wg-I, coupled by an evanescent rectangular waveguide of finite length L. This structure is often used in evanescent-mode ridged waveguide filters.
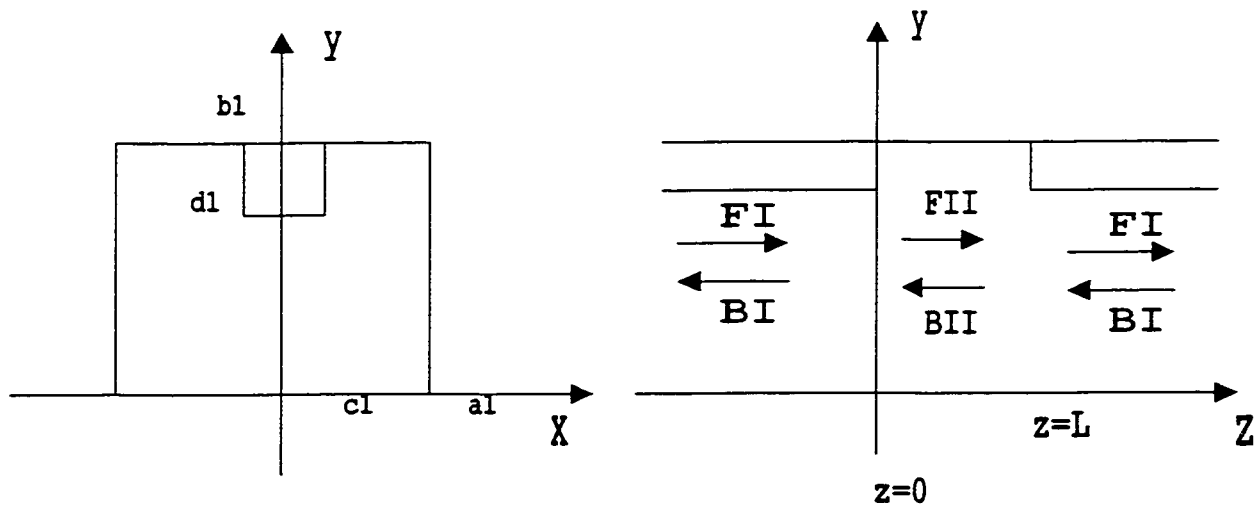
Figure 4.2.1 - Symmetrical Ridged Waveguide Coupling

For this three-dimensional microwave structure, the method described in section 4.1 can be used again to extract the overall GSM of the two-port network. However, this time the waveguide step GSM is found from the MM analysis of the symmetrical

rectangular-to-ridged waveguide step (section 3.3). For the case where the ridged waveguide is $a_1 = 0.420$", $b_1 = 0.170$", $c_1 = 0.100$" and $d_1 = 0.030$" and the rectangular waveguide is $a_1 = 0.420$", $b_1 = 0.170$" and $L = 0.150$" operating at 10 GHz, table 4.2.1 and figure 4.2.2 show the convergence of the MM-GSM method. From table 4.2.1, we can state that $|S_{11}| = 0.809$ and $|S_{21}| = 0.588$ after a maximal cutoff frequency of 220 GHz. In this case, the maximal cutoff frequency needs to be at least 20 times its operational frequency (10 GHz) in order to give three digits of accuracy.

Table 4.2.1 – S-Parameters Convergence for a Ridged Waveguide Coupling

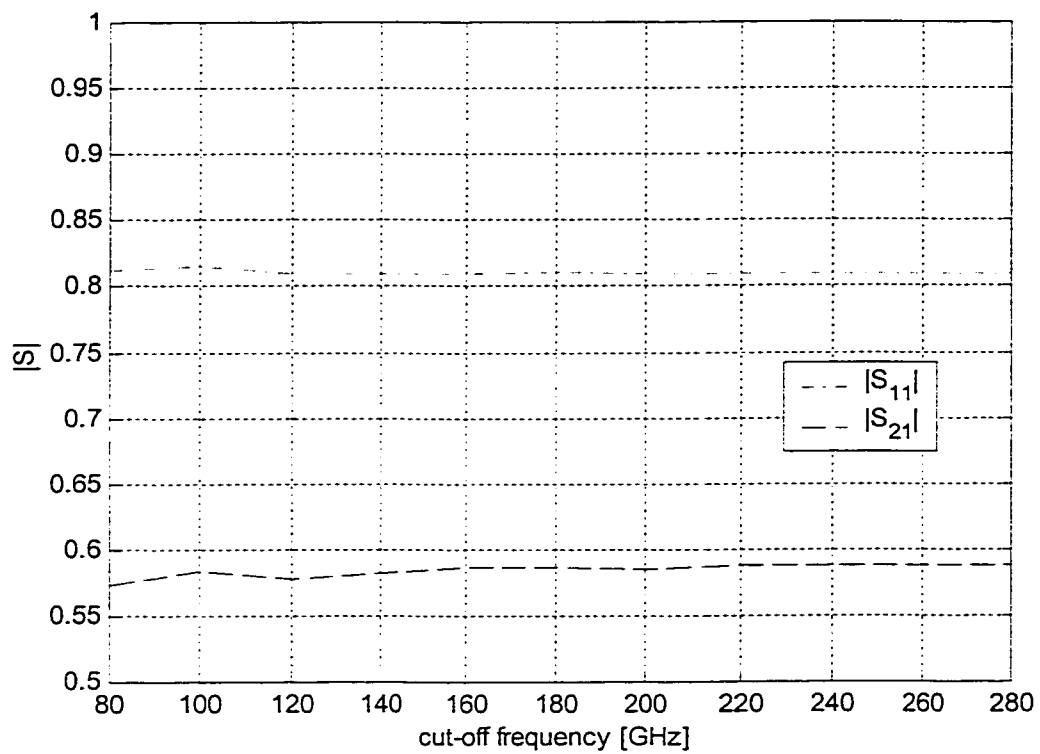| f_{cutoff} GHz	wg-I modes TE – TM	wg-II modes TE – TM	$|S_{11}|$	$|S_{21}|$
80	5 - 1	4 – 1	0.8122	0.5728
100	6 – 1	7 – 3	0.8158	0.5834
120	8 – 2	7 – 3	0.8098	0.5784
160	13 – 5	14 – 8	0.8099	0.5867
180	15 – 7	16 - 10	0.8105	0.5866
200	17 – 8	19 – 12	0.8090	0.5857
220	21 – 10	24 – 16	0.8089	0.5879
240	25 – 14	28 – 19	0.8090	0.5878
260	28 – 15	32 – 23	0.8092	0.5876
280	32 – 18	37 - 27	0.8091	0.5877

Figure 4.2.2 – S- Parameters Convergence for a Ridged Waveguide Coupling

CHAPTER 5 – CAD of the Evanescent-Mode Waveguide Filter

5.1   Evanescent-Mode Waveguide Filter

Evanescent-mode waveguide filters are often used in microwave telecommunication systems. The main advantage of this filter with respect to the other microwave filters is its wideband rejection, small size and low insertion loss. These characteristics make the evanescent-mode filter an ideal component to reject unwanted spurious and harmonic signals generated by other microwave components such as mixers and power amplifiers.

An evanescent-mode waveguide filter consists on a series of ridged waveguide resonators coupled by evanescent rectangular waveguide sections. Figure 5.1.1 illustrates a typical evanescent-mode filter to obtain a Chebyshev bandpass frequency response. Because it is often required to use standard rectangular waveguides at the input and output ports, a rectangular waveguide step is often used for the first and last coupling. In Figure 5.1.1, the microwave filter uses four distinct waveguide cross-sections, namely:

wg-O: standard rectangular waveguide;

wg-I: step transformer rectangular waveguide;

wg-II: ridge waveguide resonator;

wg-III: evanescent rectangular waveguide.

A step transformer, wg-I, is used to match the filter to the input and output rectangular waveguides. The ridged waveguide resonators, wg-II, and the evanescent rectangular waveguides, wg-III, form the filter section and they are repeated many times until enough rejection is obtained to meet the filter requirements. However, the number of resonators must be kept to a minimum in order to maintain a low insertion loss over the passband and a minimum length for the filter. Hence the necessity of a fast fullwave tool to analyze and synthesize the filter prior to its fabrication.
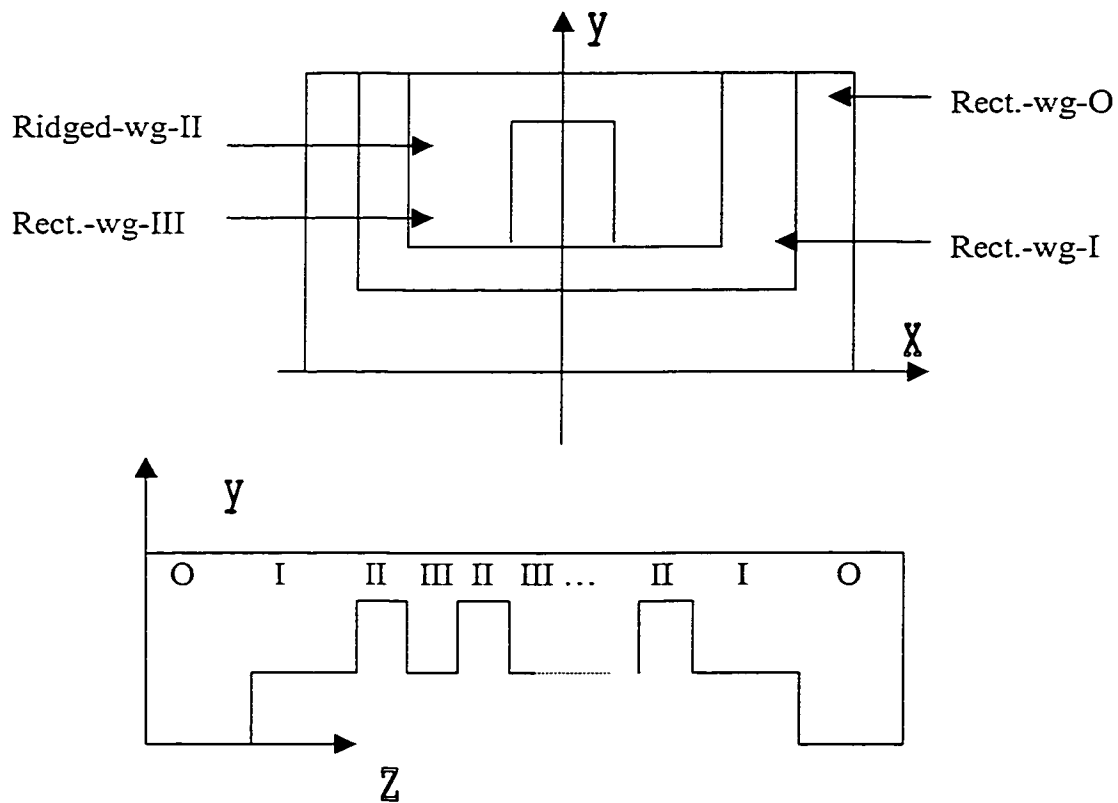
Figure 5.1.1 - Chebyshev Evanescent-Mode Waveguide Filter

The goal of this chapter is to present a fullwave analysis and synthesis method as presented in the flow chart of figure 1.1. Therefore, we will first show how to obtain the accurate and fast analysis of the evanescent-mode waveguide filter shown in figure 5.1.1 using the MM-GSM method. Second, we will demonstrate the synthesis of the evanescent-mode filter for some specific filter requirements. Finally, the results obtained with the MM-GSM method will be compared with the results measured to demonstrate the validity of the method.

5.2   Analysis of the Evanescent-Mode Waveguide Filter

The boundary conditions of the evanescent-mode waveguide filter can be decomposed into rectangular-to-rectangular waveguide steps and rectangular-to-ridged waveguide steps joined with finite length waveguides. Therefore, the MM-GSM method presented in the previous chapter to obtain the scattering parameters of the finite length rectangular iris and the ridged waveguide coupling can be extended here to predict the overall scattering phenomena of the filter.

Figure 5.2.1 is the equivalent GSM representation for the evanescent-mode waveguide filter of figure 5.1.1. In figure 5.2.1, each waveguide step is represented by its equivalent MM-GSM and each waveguide length is represented by its equivalent transmission GSM. The notation used is S_{I-II} for the MM-GSM obtained for the waveguide step between wg-I and wg-II and S^{L1}_{I} for the transmission GSM for wg-I with

length, L_1, for example. Finally, successively cascading the GSMs from left to right yields the overall GSM for the evanescent-mode filter taking into account all the waveguide modes and waveguide lengths.

$$-\boxed{S_{O\text{-}I}}-\boxed{S^{Lc1}{}_I}-\boxed{S_{I\text{-}II}}-\boxed{S^{Lr2}{}_{II}}-\boxed{S_{II\text{-}III}}- \cdots\cdots -\boxed{S^{LcN}{}_I}-\boxed{S_{O\text{-}I}}-$$

Figure 5.2.1 - Equivalent GSM Representation of the Evanescent-Mode Filter

A computer program was written in Matlab to analyze the frequency response of the evanescent-mode waveguide filter. Figure 5.2.2 shows the Graphic-User-Interface (GUI) of the program. On the left hand side, the software lets the user input the cross-section dimensions. When the *Calculate Wg Properties* button is pushed the program computes various waveguide properties such as the frequency, wavelength and impedance for the fundamental waveguide mode. On the right hand side, the user must enter the lower frequency, upper frequency and number of frequencies for the analysis in the fields denoted by *FL*, *FU*, and *#Freq*, respectively. The number of waveguide modes that will be used to calculate the filter response are entered in the fields *Fc WG-0*, *Fc WG-I* and *Fc WG-II*. As a starting guess these mode cutoff frequencies should be at least ten times greater than the cutoff frequency of the dominant mode found for the given waveguide. The rectangular waveguide lengths are entered in the field L_c and ridged waveguide lengths in L_r. Note that the first and last L_c values are the step transformer waveguide lengths whereas the other L_c values are for the evanescent rectangular waveguide lengths. When the *Analyze Filter* button is pushed, the program evaluates the

GSM for each junction, concatenates all the GSMs and find the overall GSM one frequency at the time. After the analysis the program returns a plot of the transmission loss and return loss amplitude of the filter over frequency.

Figure 5.2.1 - CAD GUI for the Evanescent-Mode Waveguide Filter

5.3   Synthesis of the Evanescent-Mode Waveguide Filter

The synthesis of a microwave filter consists on finding the waveguide dimensions in order to achieve a prescribed frequency response. Often, equivalent circuit models or experimental data are used to quickly find the unknown dimensions such as the L_c and L_r lengths of the filter. However, once the dimensions are guessed, optimization with a fullwave solver or tuning elements in the laboratory is still required.

Craven and Mok [22] were among the first to propose a lumped element circuit model to synthesize evanescent-mode waveguide filter lengths in 1971. Their work was extended by Snyder [23] in 1977. More recent synthesis models are also proposed in [24]-[26]. Today, with the advent of fast computer and electromagnetic fullwave design softwares, it is no longer necessary to spend so much time in the implementation of elaborate approximate models. This section will demonstrate how to quickly synthesize an evanescent-mode filter when a fullwave model exists.

Figure 5.3.1 shows a procedure to obtain initial filter dimensions. The procedure starts by identifying the required center frequency, f_c, filter bandwidth, bw, and passband return loss, RL, from the given filter specifications. Then, using equation (2.2.1), the minimum Chebyshev order, N, can be found in order to meet all the rejection bands. The Chebyshev order also corresponds to the number of ridged waveguide resonators required. The next step consists of determining each waveguide cross-section.

```
┌─────────────────────────────────┐
│   Determine f_c, bw and RL       │
└─────────────────────────────────┘
                │
                ▼
┌─────────────────────────────────┐
│      Find filter order, N        │
└─────────────────────────────────┘
                │
                ▼
┌─────────────────────────────────┐
│  Determine the wg O, I, II       │
│  and III cross-sections          │
└─────────────────────────────────┘
                │
                ▼
┌─────────────────────────────────┐
│  Set L_c = [ λ_g1/4 , λ_g1/4 ]   │
│  and L_r = [ 0.1 ]               │
└─────────────────────────────────┘
                │
                ▼
┌─────────────────────────┐        ┌──────────────┐
│   Run the MM-GSM solver │◄───────│  Vary L_r(1) │
└─────────────────────────┘        └──────────────┘
                │                          ▲
                ▼                          │
          ╱───────────╲        No         │
         ╱ Is resonance ╲─────────────────┘
         ╲   at f_c?    ╱
          ╲───────────╱
                │ Yes
                ▼
┌─────────────────────────────────────┐
│  Set L_c = [ λ_g1/4 , 0.1 , λ_g1/4 ]│
│  and L_r = [ L_r(1) , L_r(1) ]      │
└─────────────────────────────────────┘
                │
                ▼
┌─────────────────────────┐        ┌──────────────┐
│   Run the MM-GSM solver │◄───────│  Vary L_c(2) │
└─────────────────────────┘        └──────────────┘
                │                          ▲
                ▼                          │
          ╱───────────╲        No         │
         ╱ Is bandwidth ╲────────────────┘
         ╲    good?     ╱
          ╲───────────╱
                │ Yes
                ▼
```

Set $L_c = [\lambda_{g1}/4 \,, L_c(2) \,, L_c(2) \,, \ldots \,, L_c(2) \,, \lambda_{g1}/4 \,]$
and $L_r = [\, L_r(1) \,, L_r(1) \,, \ldots \,, L_r(1) \,]$

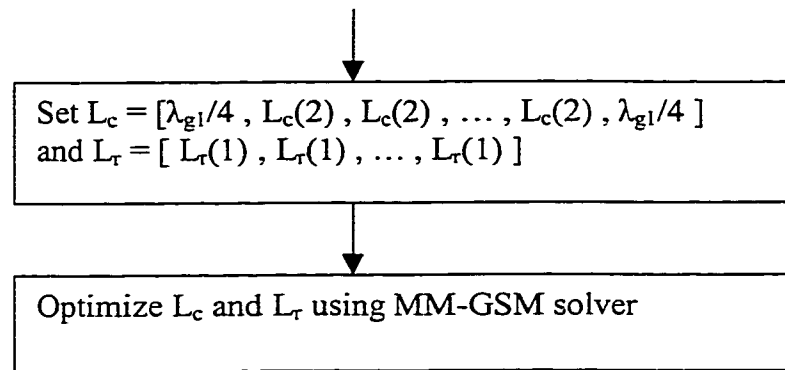Optimize L_c and L_r using MM-GSM solver
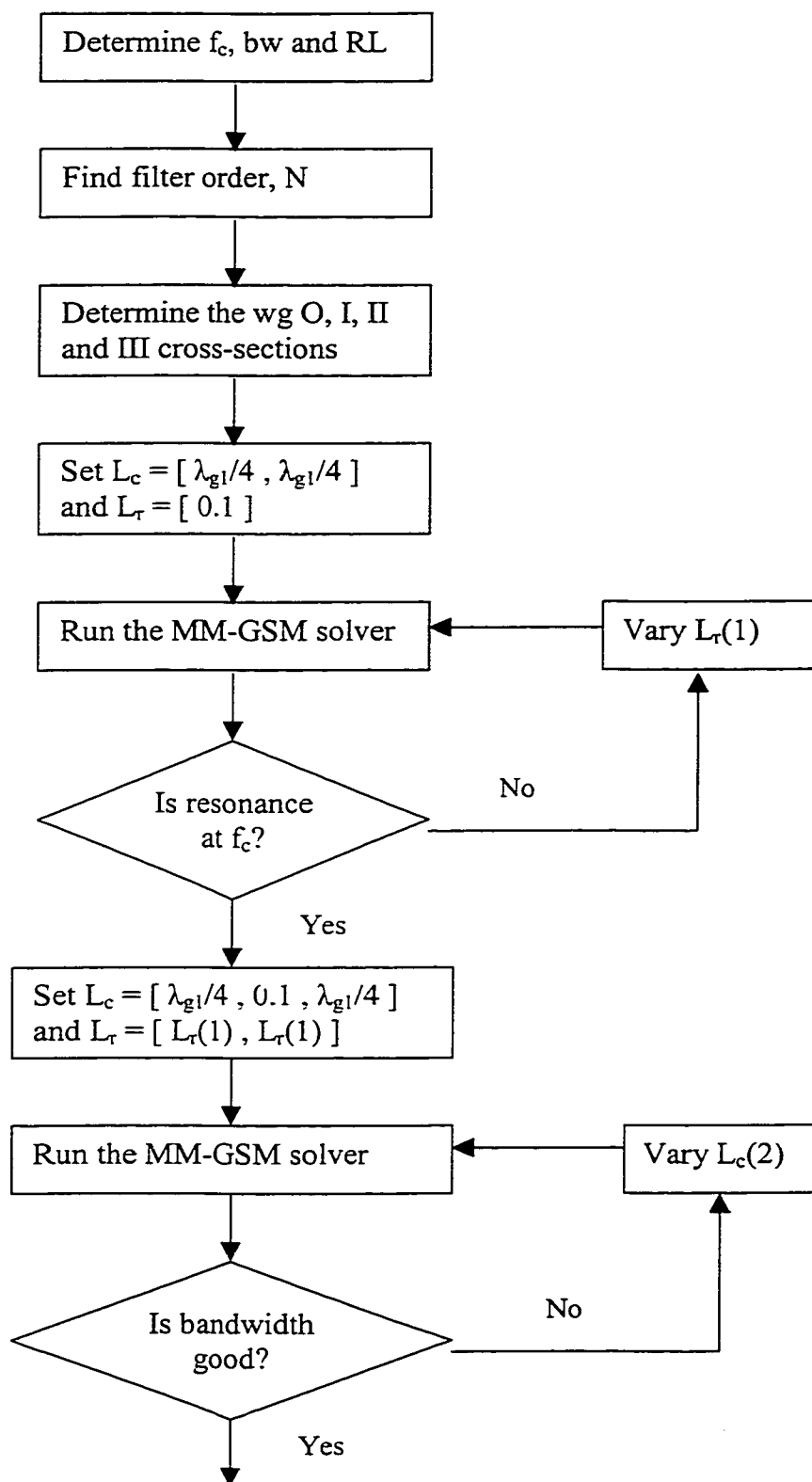
Figure 5.3.1 - Flow Chart to Synthesize an Evanescent-Mode Filter

The input and output waveguide, wg-O, is usually imposed in the filter specifications. It consists of a standard rectangular waveguide, which propagates in the fundamental mode only at the passband frequencies of the filter. The waveguide cross-sections for wg-I, wg-II and wg-III are arbitrarily chosen. However, it is required to narrow down the cross-section surface so that wg-III is evanescent at the filter passband frequencies. Once the cross-section dimensions are selected, the waveguide lengths, the N+1 L_c dimensions and the N L_r dimensions must be determined. We can start with a step transformer length of $L_c = [\ \lambda_{g1}/4 \,, \lambda_{g1}/4 \,]$ inch and a single ridged waveguide resonator of $L_r = [\ 0.1 \,]$ inch. Running the MM-GSM solver, we can find the resonance frequency of the single pole filter. The resonance frequency is the frequency at which the amplitude of the transmission is maximum as shown in figure 5.3.2. It is important to start the analysis with a wide frequency range in order to find the resonance. Once the L_r value is found for the first resonator, the frequency span can be narrowed down.
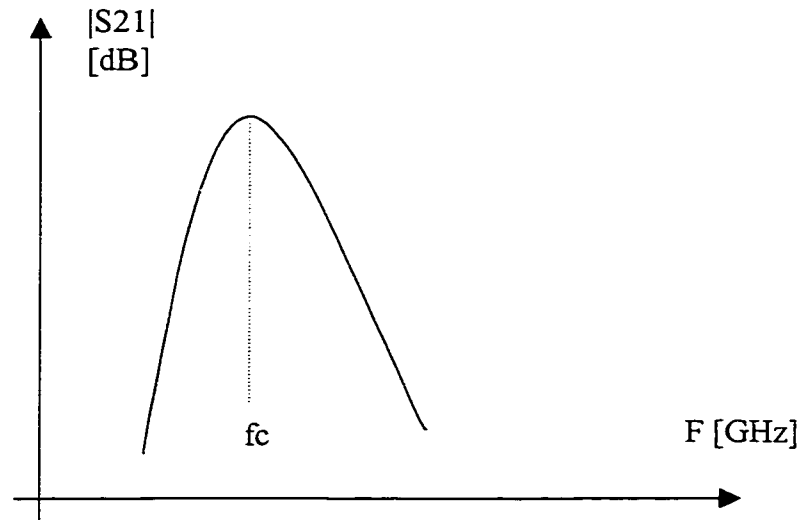
Figure 5.3.2 - Single Pole Frequency Response

The next step is to increase the number of resonators by one. For example, say that we found that L_c = [0.175 , 0.175] and L_r = [0.045], which produces a resonance at a frequency of 22 GHz. Now, we must arbitrarily choose the length of the evanescent rectangular waveguide, wg-III, to give the appropriate coupling between the two resonators. We can start with a guess length of 0.1 inch. Therefore, L_c = [0.175 , 0.1 , 0.175] and L_r = [0.045 , 0.045] and we run the solver. The transmission response of the two-pole filter will look like the curve show in Figure 5.3.3. Now, the length of the evanescent rectangular waveguide must be set such that the bandwidth of the two resonances is approximately equal to bandwidth of the filter. Lets say that L_c = [0.175 , 0.075 , 0.175] and L_r = [0.045 0.045] were found. Then, the remaining step in the filter synthesis is to set the L_c vector to N+1 elements and the L_r vector to N elements using the $L_c(2)$ and $L_r(1)$ values found in the previous steps. For example, if a fourth order Chebyshev filter is necessary to meet the requirements, then, L_c = [0.175 , 0.075 , 0.075 ,

0.075 , 0.175] and L_r = [0.045 , 0.045 , 0.045 , 0.045]. At this stage, all the filter

lengths are guessed. The dimensions can be optimized using the MM-GSM solver until
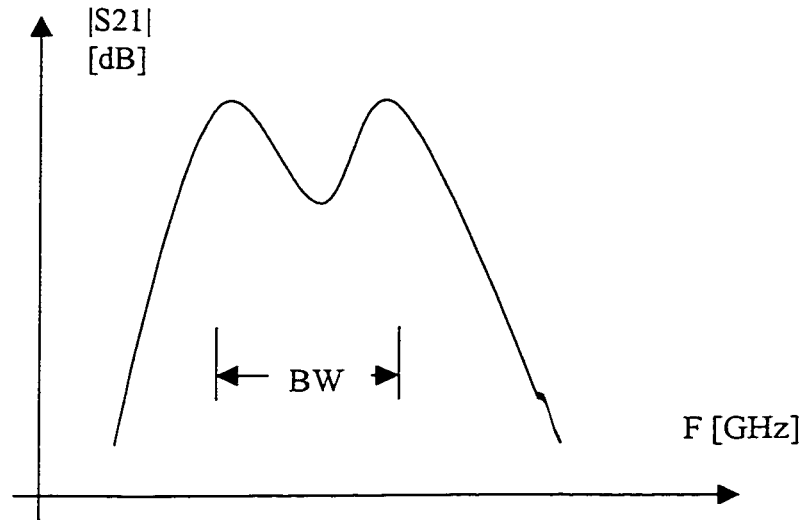
all requirements are met.

Figure 5.3.3 – Two-Pole Frequency Response

5.4 Design Example

In order to verify the accuracy of the MM-GSM method, an evanescent-mode

waveguide filter was designed. The evanescent-mode waveguide filter requirements are:

Return Loss > 20 dB for 19.5 to 21 GHz

Rejection > 30 dB for 29.5 to 31.5 GHz

I/p and O/p interface: WR42

The synthesis method explained in section 5.3 was used to find the waveguide cross-sections and lengths. The waveguide lengths were then optimized using the simplex method, an optimization routine that comes with the Matlab optimization toolbox. Figure 5.2.1 shows the waveguide dimensions obtained after synthesis and optimization. Figure 5.4.1 shows the filter response of the evanescent-mode waveguide filter using the MM-GSM solver. The analysis takes 46 seconds for 51 frequency points using a Pentium II 350 MHz processor. During the optimization, only 11 points were used which reduces the optimization time considerably.
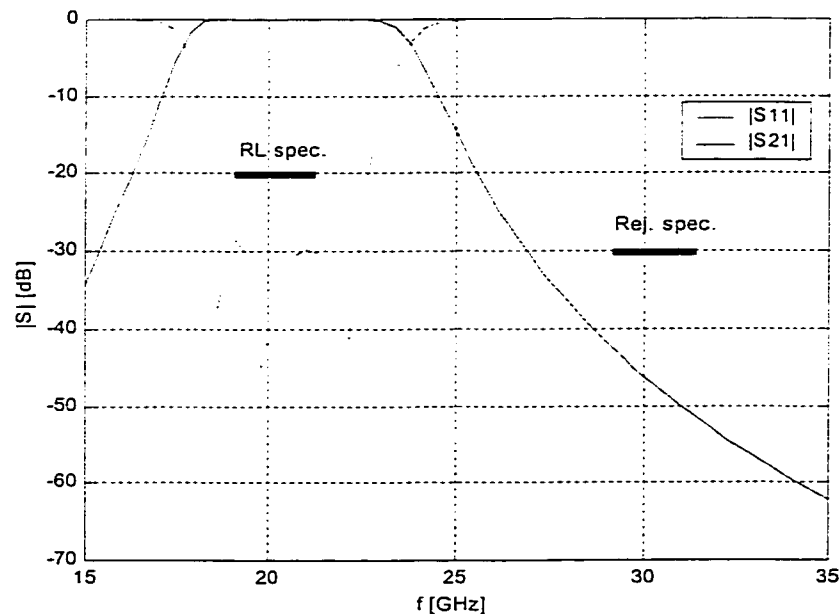

Figure 5.4.1 - MM-GSM Solver Frequency Response

Figure 5.4.2 shows two evanescent-mode waveguide filters that were built to the dimensions found by the MM-GSM method. The two filters are made of aluminum and

are approximately 1.5 inch long. No tuning screws are used to compensate the frequency
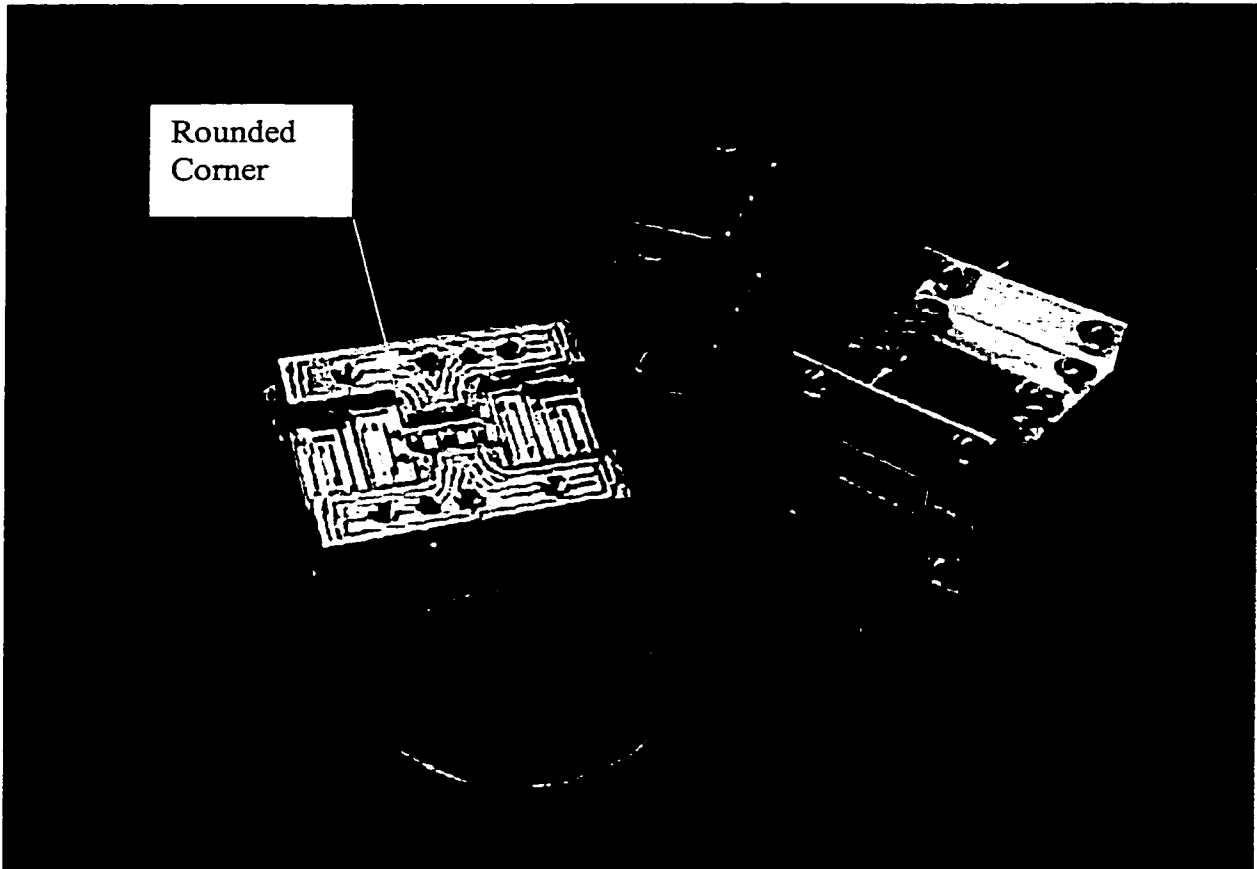
response of the filter.

Figure 5.4.2 - Evanescent-Mode Waveguide Filters

Figure 5.4.3 compares the simulated data against the measured data. The

measured results are slightly shifted up in frequency, but the filter still meets the

requirements without tuning. The shift in frequency can be explained by the tolerance of

the machining. The effect of the rounded corners in the step transformer due to

machining can also explain the mismatch in the return loss, which causes one of the poles

to be detuned in the measurement. The measured data over 25 GHz seems to ripple. This is due to the use of WR28 to WR42 tapers used to make the transmission measurement from 25 GHz to 40 GHz.
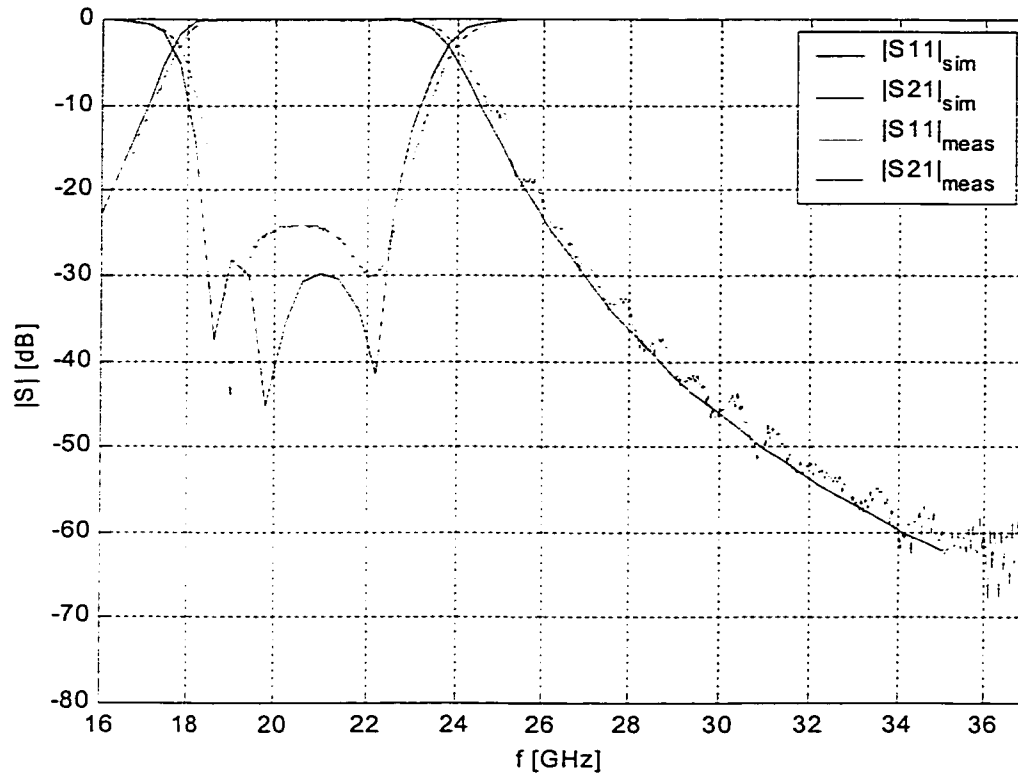

Figure 5.4.3 - Simulation vs. Measurement

Figure 5.4.4 explains the discrepancy between the simulated and measured data. The values of L_c, L_r and D (ridge waveguide gap) were randomly varied within the machining tolerance of $\pm$ .0005 inch. The blue curves represent the simulated filter responses whereas the red curve is still the measured data. This proves that the program developed predicts accurately the filter response, but margin must be set in the design in order to meet the filter requirements.

The measured filter is also detuned in the passband as shown in figure 5.4.3 and the detuning cannot be explained by the worst-case analysis in figure 5.4.4. The return loss discrepancy is probably due to poor cover-to-body grounding. This phenomena is difficult to simulate by computer, but at high frequency such has 22 GHz, a very small leak in the assembly can lead to the failure of the filter. This problem is often remedied by adding more assembly screws or adding silver epoxy. Another phenomena that can explain the mismatch in the return loss is the effect of rounded corners in the step transformer as shown in figure 5.4.2. Rounded corners are required in the machining of the filter body to include the radius of the milling tool. Often, we try to minimize the radius so that the rounded corners are assumed negligible. To include these rounded corners in the solver using the MM-GSM method, many rectangular-to-rectangular waveguide steps can be used to approximate the corner as shown in figure 5.4.5. Then, using the MM-GSM method, the accurate S-parameters of the corner can be included in the solver.
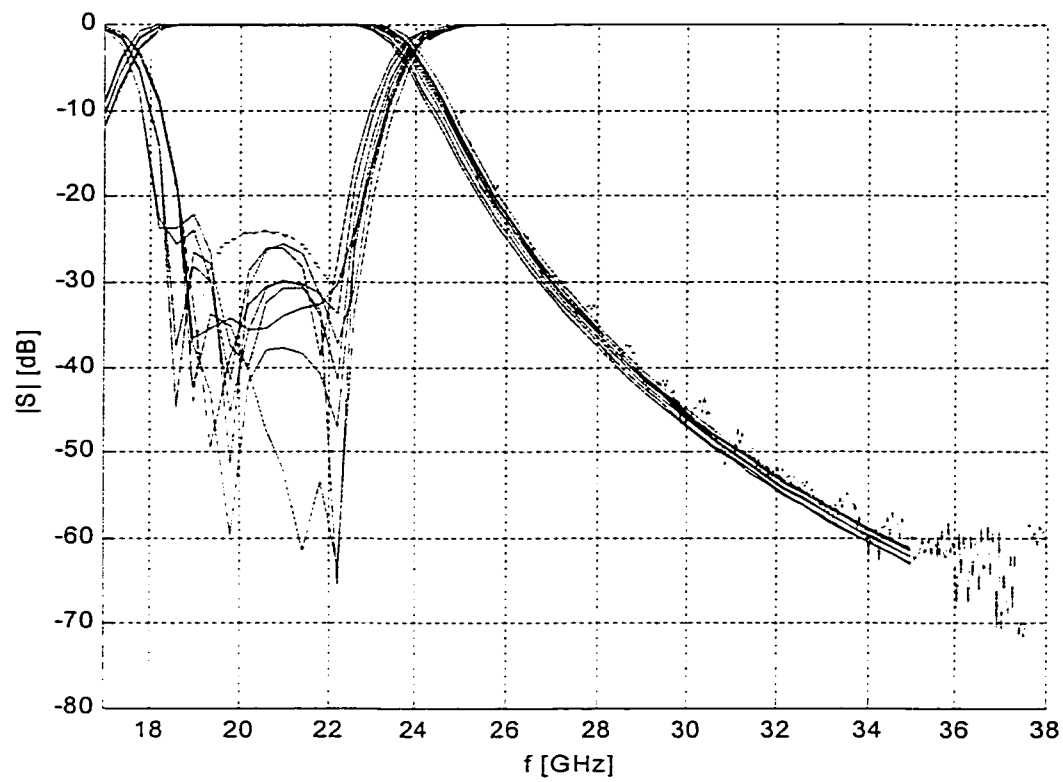
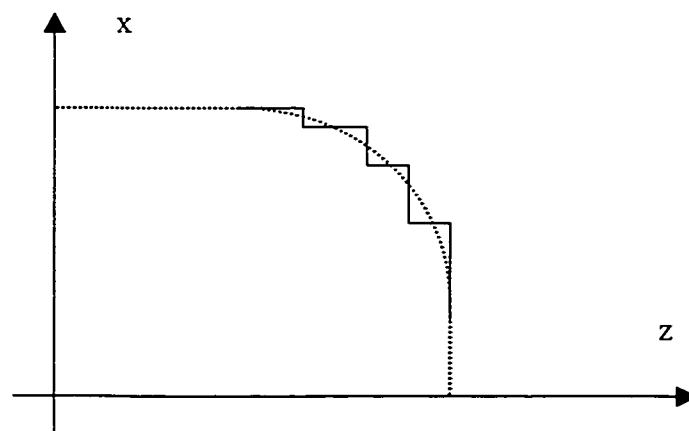**Figure 5.4.4** – Simulation Worst Case Analysis.

Figure 5.4.5 – Rounded Corners Approximation by MM-GSM Method

CHAPTER 6 – Conclusion

In this thesis, the basic microwave filter theory was introduced. First, the ideal filter response was characterized. Then, a Chebyshev approach was presented to approximate the ideal filter response. Using the Chebyshev polynomial function and the passband and ripple requirements of the filter, it was shown how to find the minimum filter order and still meet the rejection requirements. Once the order of the filter was found, a two-port network with the same number of resonators as the order of the filter can be synthesized. It was shown that the Chebyshev prototype can be used to extract the dimensions for a direct-coupled-resonator network. A direct-coupled circuit is composed of waveguide resonators coupled inline by evanescent waveguide sections. The coupling between the resonators can be modeled as impedance inverters, which simulates the evanescent field coupling between the microwave resonators. Converting the impedance network model information into waveguide physical dimensions through experimental data is the traditional way to synthesize microwave filters. However, this method is only accurate for narrow band filters since the dimensions can be evaluated at a single frequency only. As we deviate from this frequency, the matching between the impedance network model and the direct-coupled microwave filter becomes more and more erratic. Hence, the advantage of using a fullwave numerical model to synthesize the microwave filter. The fullwave solver rigorously computed all the electromagnetic fields inside the filter at a given frequency including all its boundary conditions and finite lengths. If enough discretization is used, the fullwave model predicts the exact frequency response of the filter.

To demonstrate the advantages of using a fullwave solver, the MM-GSM method was presented to analyze 3-D structures composed of rectangular and ridged waveguide sections. The MM method is a popular numerical method for the field analysis between two dissimilar waveguide discontinuities. The method consists of first finding the modes in each waveguide. The fields in the waveguides are then expanded as the sum of all mode functions with unknown forward and backward amplitude coefficients. By matching the tangential electromagnetic fields at the junction of the two waveguides and isolating for the unknown forward and backward coefficients, the GSM of the waveguide step was derived. If all the modes (i.e., infinite modes) are used, the MM analysis would compute the exact GSM to the problem. Since it is impossible to use an infinite number of terms in the computation of the GSM waveguide step, the result is an approximation to the exact solution. However, it starts to converge to the exact solution after a few modes only. Two examples were analyzed using MM, namely, the rectangular-to-rectangular waveguide step and the rectangular-to-ridged waveguide step.

Most of microwave passive components such as evanescent-mode waveguide filters can be decomposed into segments of dissimilar waveguides. For such components, it was shown how to concatenate all the GSMs to extract the overall GSM of the microwave component. First, the GSM for each waveguide junction was computed using the MMM. Then, all waveguide step GSMs where interconnected with waveguides GSM to include the finite length of the waveguides. Finally, the overall GSM was obtained by successively cascading the GSMs from left to right. Two example of microwave structures were given, the rectangular waveguide iris and the ridged waveguide coupling.

These structures are often used to build microwave component such as couplers and filters. For both problems, it was found that the S-parameters converge to at least three significant digits using a maximal cutoff frequency of 20 times the operational frequency.

After introducing the MM-GSM method, a CAD program was presented to solve for scattering parameters of the evanescent-mode waveguide filter. This filter consists on ridged waveguide resonators coupled by evanescent rectangular waveguides. Using the MM-GSM solver, a synthesis method to arrive at initial filter dimensions was described. These dimensions can then be optimized using the solver to meet the filter requirements.

In order to verify the accuracy of the MM-GSM solver, an evanescent-mode waveguide filter was designed, built and tested. The results measured were in agreement with the solver simulations and compliance of the filter was obtained without the use of tuning screws. However, the measurements showed that the filter was slightly shifted in frequency and the return loss was slightly detuned. A worst-case analysis was done and the results obtained showed that the frequency shift was probably due to the machining tolerances. However, the worst-case analysis did not prove the return loss mismatched in the passband. The mismatch in the passband was probably due to machining rounded corners or poor assembly contact between the body and cover.

The evanescent-mode waveguide filter that was designed could have better performance (i.e., closer to the simulated data) if tighter machining tolerances were imposed. However, imposing very precise machining leads to a much higher cost to

fabricate the filter. The assembly body-to-cover grounding is difficult to control and predict. However, better surface finish, more assembly screws and silver epoxy are three possible ways to counter this problem. Finally, it was shown how to include the rounded corner into the MM-GSM solver. The method consists of approximating the rounded corners in terms of many rectangular–to-rectangular waveguide steps. Adding this boundary condition to the MM-GSM solver would make the solver more rigorous. Besides adding the rounded corner to the solver, another interesting feature that would enhance the CAD tool would be to include the losses due to the finite conductivity of the metal. These two features are topics that can be explored in future work.

REFERENCES

[1]   Nathan Marcuvitz, 'Waveguide Handbook', M.I.T. Rad. Lab. Series, vol. 10, McGraw-Hill, New York, 1951, pp.217-334.

[2]   G. Matthaei, L. Young, E.M.T. Jones, 'Microwave Filters, Impedance-Matching Networks, and Coupling Structures', McGraw-Hill, New York, 1964.

[3]   R. Sorentino, 'Numerical Methods for Passive Microwave and Millimeter Wave Structures', IEEE Press, N.Y., 1989, Part 1.

[4]   T. Itoh, 'Numerical Techniques for Microwave and Millimeter-Wave Passive Structures', John Wiley & Sons, N.Y., 1989.

[5]   J. B. Davies, C.A. Muilwyk, 'Numerical Solution of Uniform Hollow Waveguides with Boundaries of Arbitrary Shapes', Proc. IEE, vol. 113, Feb. 1966.

[6]   P.P. Silvester, R.L. Ferrari, 'Finite Elements for Electrical Engineers', Cambridge University Press, New York, 1983.

[7]   A. Wexler, 'Solution to Waveguide Discontinuities by Modal Analysis', IEEE MTT-15, Sep. 1967, pp. 508-517.

[8]   Roger F. Harrington, 'Field Computation by Moment Methods', Macmillan, New York, 1968.

[9]   K.S. Yee, 'Numerical Solution of Initial Boundary Value Problems Involving Maxwell's Equations in Isotropic Media', IEEE Trans. Antennas Propagation, vol. 14, May 1966, pp. 302-307.

[10]   P.B. Johns, R.L. Beurle, 'Numerical Solution of Two-dimensional Scattering Problems Using Transmission-line Matrix', Proc. Inst. Electr. Eng., vol. 118, Sep. 1971, pp. 1203-1208.

[11]   H. Patzelt, F. Arndt, 'Double-Plane Steps in Rectagular Waveguides and their Application for Transformers, Irises, and Filters', IEEE MTT-30, May 1982, pp.771-776.

[12]   J. Bornemann, F. Arndt, 'Model S-Matrix Design of Optimun Stepped Ridged and Finned Waveguide Transformers', IEEE MTT-35, June 1987, pp. 561-567.

[13]   R. Schaumann, M. S. Ghausi, K. R. Laker, 'Design of Analog Filters', Prentice Hall, New Jersey, 1990

[14] S. B. Cohn, *'Direct-Coupled-Resonator Filters'*, Proc. IRE, Vol. 45, February 1957, pp. 187-196.

[15] J. Uher, J. Bornemann, U. Rosenberg, *'Waveguide Components for Antenna Feed Systems: Theory and CAD'*, Artech House, Norwood, 1993.

[16] H. Schmiedel, F. Arndt, *'Field Theory Design of Rectangular Waveguide Multiple-Slot Narrow Wall Couplers'*,IEEE Trans. MTT, vol. 34, July 1986, pp. 791-798.

[17] X.P. Liang, K.A. Zaki, *'Modelling of Cylindrical Dielectric Resonators in rectangular Waveguides and Cavities'*, IEEE Trans. MTT, vol. 41, Dec. 1993, pp. 2174-2180.

[18] G. Kowalski, R. Pregla, *'Dispersion Characteristics of Shielded Microstrips with Finite Thickness'*, Arch. Elek. Ubertragung, vol. 25, Apr. 1971, pp. 193-196.

[19] J.P. Montegomery, *'On the Complete Eigenvalue Solution of Ridged Waveguide'*, IEEE Trans. MTT, vol. 19, June 1971, pp. 547-555.

[20] Y. Utsumi, *'Variational Analysis of Ridged Waveguide Modes'*, IEEE Trans. MTT, vol. 33, Feb. 1985, pp. 111-120.

[21] J. Bornemann, F. Arndt, *'Transverse Resonance, Standing Wave, and Resonator Formulations of the Ridge Waveguide Eigenvalues Problem and Its Application to the Design of E-plane Finned Waveguide Filters'*, IEEE Trans. MTT, vol. 38, Aug. 1990, pp.1104-1113.

[22] G.F. Craven, C.K. Mok, *'Design of Evanescent-Mode Waveguide Bandpass Filter for a Prescribed Insertion Loss Characteristic'*, IEEE Trans. MTT, vol. 19, March 1971, pp. 295 − 308.

[23] R.V. Snyder, *'New Application of Evanescent-Mode Waveguide to Filter Design'*, IEEE Trans. MTT, vol. 25, Dec.1977, pp. 1013 − 1021.

[24] H.F. Chappell, *'Waveguide Lowpass Filter Using Evanescent Mode Inductors'*, Microwave Journal, vol. 2A, Dec. 1978, pp. 71-72.

[25] A.M.K. Saad, *'Novel Lowpass Harmonic Filters for Satellite Application'*, IEEE Trans. MTT-S, Dec. 1984, pp. 292-294.

[26] J.C. Nanan et al., *'A Two Step Synthesis of Broadband Ridged Waveguide Banpass Filters with Improved Performances'*, IEEE Trans. MTT, vol. 39, Dec. 1991, pp. 2192 − 2197.